JCIM JOURNAL OF CHEMICAL INFORMATION AND MODELING

pubs.acs.org/jcim Article

Mutation-Induced Impacts on the Switch Transformations of the GDP- and GTP-Bound K-Ras: Insights from Multiple Replica Gaussian Accelerated Molecular Dynamics and Free Energy Analysis

Jianzhong Chen,* Shaolong Zhang, Wei Wang, Laixue Pang, Qinggang Zhang, and Xinguo Liu*

Cite This: J. Chem. Inf. Model. 2021, 61, 1954−1969 Read Online

ACCESS | Metrics & More | Article Recommendations | Supporting Information

ABSTRACT: Mutations yield significant effect on the structural flexibility of two switch domains, SW1 and SW2, in K-Ras, which is considered as an important target of anticancer drug design. To unveil a molecular mechanism with regard to mutation-mediated tuning on the activity of K-Ras, multiple replica Gaussian accelerated molecular dynamics (MR-GaMD) simulations followed by analysis of free energy landscapes (FELs) are performed on the GDP- and GTP-bound wild-type (WT), G12V, and D33E K-Ras. The results suggest that G12V and D33E not only evidently change the flexibility of SW1 and SW2 but also greatly affect correlated motions of SW1 and SW2 separately relative to the P-loop and SW1, which exerts a certain tuning on the activity of K-Ras. The information stemming from the analyses of FELs reveals that the conformations of SW1 and SW2 are in high disorders in the GDP- and GTP-associated WT and mutated K-Ras, possibly producing significant effect on binding of guanine nucleotide exchange factors or effectors to K-Ras. The interaction networks of GDP and GTP with K-Ras are identified and the results uncover that the instability in hydrogen-bonding interactions of SW1 with GDP and GTP is mostly responsible for conformational disorder of SW1 and SW2 as well as tunes the activity of oncogenic K-Ras.

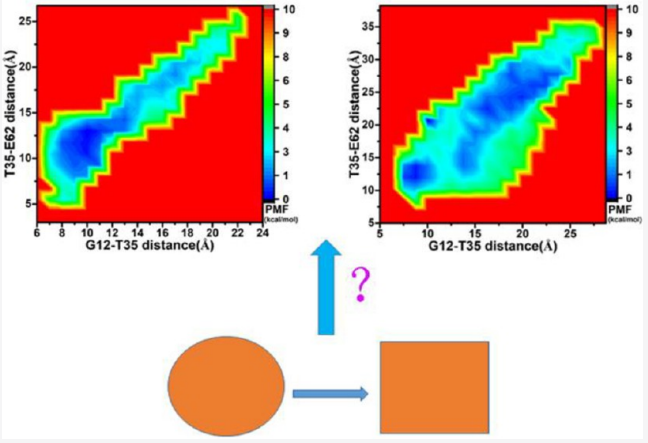

INTRODUCTION

It is well-known that molecular switches play a significant role in identification of receptors on ligands and conformational transformations of receptors. Small and monomeric GTPase proteins functionally act as a molecular switch in intracellular signaling pathways, being responsible for the regulation of cell growth and differentiation.[1−4] The currently detected GTPase proteins are mainly classified into three main family groups of H-Ras, K-Ras, and N-Ras.[5] These Ras proteins not only share highly similar topology structures but also feature an interconversion cycle between the active state of the GTP-bound Ras proteins and the inactive state of the GDP-associated ones.[6−8] Through this cycle, the GTP is hydrolyzed into the GDP, and two switch domains (SW1 and SW1) endure big conformational alterations.[9] Recently, increasing attentions are paid to these Ras proteins because of their close relations to a variety of human cancers.[10−13] Multiple literatures verify that mutation-mediated activity of Ras proteins have been frequently found in cancer patients, of which K-Ras attracts special interests in insights into possible strategies of cancer treatments.[14−19] Unfortunately, efficient inhibitors toward K-Ras are clinically unavailable by now. Therefore, K-Ras has been regarded as a significant and promising target of anticancer drug design and development.

Multiple reports reveal that mutations highly affect the conformational changes of two switches SW1 and SW2, in which SW1 is involved in residues 25−40 and SW2 consists of residues 60−76,[20−22] and P-loop is another significant conformational feature in the secondary structures of K-Ras (Figure 1A). Two switch domains, SW1 and SW2, together with the P-loop shape a binding pocket of guanine nucleotide exchange factors (GNEFs) or effectors (Figure 1B). The literature indicates that mutations of oncogenic K-Ras have a vital effect on the conformational transformation of SW1 and SW2, which further disturbs binding of GNEFs or effectors and tunes the activity of K-Ras.[23−25] Based on oncogenic roles of K-Ras, different works have been involved in insights into mutation-mediated conformational transformations of K-

Received: December 22, 2020
Published: March 19, 2021

https://doi.org/10.1021/acs.jcim.0c01470
J. Chem. Inf. Model. 2021, 61, 1954−1969

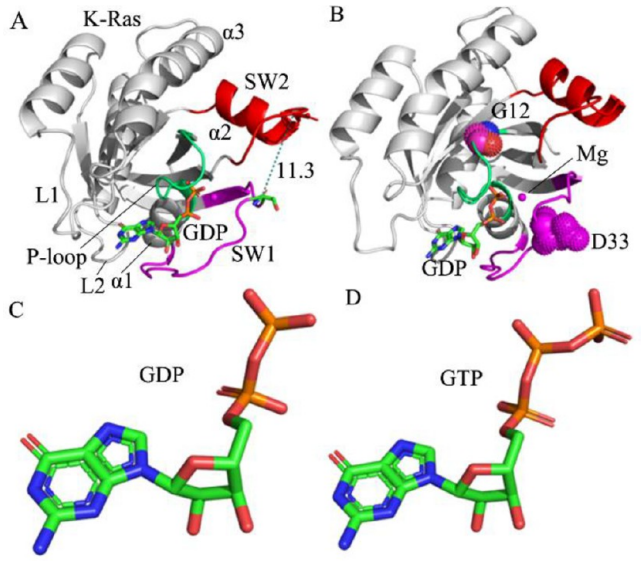

Figure 1. Molecular structures: (A) the GDP-bound K-Ras, in which K-Ras is shown in cartoon modes and two significant switch domains SW1 and SW2 are individually displayed in magentas and red, (B) mutated sites, from which two mutated residues G12 and D33 are shown in ball modes, (C) GDP, and (D) GTP. In this panel, GDP and GTP are exhibited in stick styles and magnesium ion (Mg) is depicted in ball patterns.

Ras,[20,26−28] phosphorylation-induced effect on the activity of K-Ras,[29−32] bindings of K-Ras to membranes,[33−36] and allosteric drug design toward K-Ras.[37−39] These studies have provided rational and useful information for the understanding of the roles of K-Ras in anticancer treatment. However, it is still highly essential to deeply decrypt mutation-mediated influences on conformational transformations of SW1 and SW2 for development of anticancer drugs targeting oncogenic K-Ras mutations.

To date, various experimental works have focused on mutation-induced impacts on conformational changes of the GTP- and GDP-bound K-Ras and have obtained X-ray crystal and NMR structures of K-Ras,[10,20,38,40,41] which provide reliably structural bases for accurately understanding the target roles of oncogenic K-Ras mutants in anticancer treatment. For instance, Bera et al. report a crystal structure of the GDP-associated V14I K-Ras at 1.5−1.6 Å resolution and their study reveals a marked extension of switch 1 away from the G-domain and nucleotide-binding site of K-Ras.[42] Cruz-Migoni et al. apply new crystallization conditions to refine the structure of the Q61H K-Ras complexed with the GTP-analog GppNHp and their structure is suitable for soaking with compounds, moreover they identify several potent compounds that can inhibit the activity of K-Ras.[26] A structure of the GppNHp-bound G13D K-Ras determined by Johnson et al. not only uncovers that the G13D K-Ras possesses a unique destabilization of the nucleotide binding pocket but also verifies that the G13D K-Ras has an attenuated oncogenic phenotype by comparison with the G12D K-Ras.[28] More fortunately, small molecules covalently bonding with K-Ras create binding sites and inhibit the activity of Ral GTPases.[43−45] These findings contribute a favorable molecular basis and conformational information for design of clinically available inhibitors toward oncogenic K-Ras mutants.

Although experimental works provide valuable structural bases, they also miss key dynamics information on conformational changes, which is highly significant for drug design. To overcome this shortcoming, a great many computation and simulation technologies, such as conventional molecular dynamics (cMD),[46−55] free energy landscapes (FELs),[56−58] metadynamics,[59,60] essential dynamics (ED) analysis,[61] accelerated molecular dynamics (aMD),[62,63] and Gaussian accelerated molecular dynamics (GaMD),[64−68] etc., are developed to obtain rational dynamics information concerning conformational alterations of proteins. Furthermore, these technologies have been successfully applied to decode mutation-induced conformational changes and activity adjustment of K-Ras and other Ras proteins.[27,69−72] For example, Lu et al. performed exchanged nucleotide simulations, and their results unveiled that conformational transformation is more accessible in the GTP-to-GDP exchanges than in the GDP-to-GTP one.[73] Our previous insights into the mutation-mediated effect on conformational changes of the GppNHp-bound H-Ras reveal that mutations G12V, T35S, and Q61K greatly affect the switch transformation of SW1 and SW2.[74] Gorfe et al. investigated the dynamics behavior of Ras proteins using cMD simulations and principal component analysis, and their results uncover that the inactive-to-active transition of Ras proteins involves a multiphase process formed by the relative rearrangement of two switches and the orientation of Tyr32.[75] Although these theoretical works have provided some details concerning the conformational alterations of the GTP-, GDP-, and GppNHp-bound K-Ras, it is still of high significance for design of anticancer drugs to deeply reveal the energy basis relating to the conformational changes of K-Ras due to mutations.

Two guanosine phosphates, GTP and GDP, share a highly similar structure (Figure 1, parts C and D). The GTP carries four net negative charges, while the GDP has three ones. The changes of electrostatic environment caused by the exchange of the GTP into GDP possibly bring different impacts on conformational changes of K-Ras, on the other hand, mutations also possibly affect bindings of the GTP and GDP to K-Ras. The clarification of these issues may be helpful for the understanding of drug design toward K-Ras. With this aim, the GTP, GDP and two mutations, G12V and D33E, are selected to decipher energy basis affecting bindings of the GTP and GDP to K-Ras. G12V is involved in a change of the hydrophobic side chain in G12 while D33E induces an alteration of the polar side chain in D33; hence, the electrostatic property changes caused by G12V and D33E certainly affect binding of GTP and GDP to K-Ras, which is the reason we selected these two mutants. To realize the current aim, multiple replica GaMD simulation, an extensively used sampling technology, is coupled with FELs and essential dynamics (ED) analysis to perform this study. We expect that this work can reach three aims as follows: (1) probing conformational changes of the GTP- and GDP-bound K-Ras because of two mutations, G12V and D33E, (2) revealing the energetic basis of the mutation-dependent conformational changes of K-Ras, and (3) shedding light on the mutation-mediated influences on the interaction networks of GTP and GDP with K-Ras.

MATERIALS AND METHODS

Constructions of Simulated Systems. The initial atomic coordinates of the GDP-bound wild-type (WT) K-Ras are

https://doi.org/10.1021/acs.jcim.0c01470
J. Chem. Inf. Model. 2021, 61, 1954−1969

extracted from the crystal structure (5W22)[76] arising from the Protein Data Bank (PDB). Due to the missing of residues in the crystal structure of the GTP-bound WT K-Ras (5VQ2),[76] the structure of the GTP-associated WT K-Ras is obtained by removing the GDP and incomplete K-Ras from the superimposed structures of 5W22 with 5VQ2. To keep atomic coordinate consistence, the GDP-bound G12V and D33E K-Ras are generated by individually changing G12 and D33 of the GDP-associated WT K-Ras into V12 and E33 with the Leap module in Amber 18,[77,78] while the GTP-bound G12V and D33E K-Ras are produced by separately mutating G12 and D33 in the GTP-associated WT one into V12 and E33. The magnesium ion (Mg^{2+}) in the crystal structure is retained at the initial model. The protonated states of residues in K-Ras are assigned by using the program H++ 3.0.[79] All force field parameters used in the current work are derived by utilizing the Leap module in Amber[77,78] according to the procedure as follows: (1) the missing hydrogen atoms in the crystal are bonded to the corresponding heavy atoms, (2) the parameters of the WT and mutated K-Ras are assigned by the aid of the ff14SB force field,[80] (3) the parameters of GTP and GDP arise from the work of Meagher et al.,[81] (4) an octahedral periodic box of water with a buffer of 12.0 Å consisting of ∼9000 water molecules is constructed to solve each compound and the force field parameters of water molecules stem from the TIP3P model,[82] and (5) the appropriate number of sodium ions (Na^+) is added around each complex to build a neutral simulated system, in which the parameters of Na^+ and Mg^{2+} stem from the Aqvist force field.[83]

Multiple Replica Gaussian Accelerated Molecular Dynamics. To explore the effect of G12V and D33E on the conformational changes of the GTP- and GDP-bound K-Ras, MR-GaMD simulations of four replicas are carried out to efficiently improve conformational samplings of K-Ras. The scheme of MR-GaMD simulations is as below: (1) a 30000-step steepest descent minimization followed by 3000-step conjugate gradient minimization is run to remove high energy contacts between atoms, (2) a softly heating procedure of 1 ns in the *NVT* condition is performed to enhance the temperature of each simulated systems from 0 to 310 K, (3) a equilibrated procedure in 310 K and the *NPT* ensemble is conducted to further equilibrate each simulated system, (4) a cMD of 200 ns is executed to relax each system without restriction at constant temperature of 310 K and pressure of 1 bar, (5) three conformations are randomly extracted from the above cMD simulation and the initial atomic velocities are assigned to these three conformation with the Maxwell distribution to restart three cMD simulations, and (6) the ending structures from the aforementioned fourth and fifth phases are used as the initial structures of MR-GaMD simulations of four replicas with the total simulation time of 2.4 μs, from which the MR-GaMD of each replica is run for 600 ns.

During GaMD simulations, a harmonic boost potential is adopted to cut down free energy barriers of the simulated systems and enhance conformational samplings. In general, if $V(\vec{r})$ is lower than a threshold energy E, the potential energy $V(\vec{r})$ of the system is updated as $V^*(\vec{r})$ by the aid of eqs 1 and 2

$$V^*(\vec{r}) = V(\vec{r}) + \Delta V(\vec{r}) \tag{1}$$

$$\Delta V(\vec{r}) = \begin{cases} 0 & V(\vec{r}) \geq E \\ \frac{1}{2}k(E - V(\vec{r}))^2, & V(\vec{r}) < E \end{cases} \tag{2}$$

from which k denotes the harmonic force constant, while the parameters E and k can be adjusted by adhering to three enhanced sampling principles determined through eqs 3 and 4 as follows

$$V_{\max} \leq E \leq V_{\min} + \frac{1}{k} \tag{3}$$

$$\mathrm{k} = k_0 \frac{1}{V_{\max} - V_{\min}} \tag{4}$$

in which if E is set as the lower bound $E = V_{max}$, then k_0 is determined with the eq 5

$$k_0 = \min\left(1.0, \frac{\sigma_0}{\sigma_V} \cdot \frac{V_{\max} - V_{\min}}{V_{\max} - V_{avg}}\right) \tag{5}$$

on the contrary, if E is set as the upper bound $E = V_{min} + 1/k$, then k_0 is derived from the eq 6

$$k_0 = \left(1.0 - \frac{\sigma_0}{\sigma_V}\right) \cdot \left(\frac{V_{\max} - V_{\min}}{V_{avg} - V_{\min}}\right) \tag{6}$$

where V_{max}, V_{min}, and V_{avg} indicates the minimum, maximum, and averaged potential energies of the simulated systems, separately. The parameter σ_V is standard deviation of the system potential energies, while the parameter σ_0 is a user-determined upper limit for accurately reweighting. For this study, 2.4-μs MR-GaMD simulations, consisting of four-replica GaMD simulations of 600 ns, are performed on the GTP- and GDP-bound WT and mutated K-Ras, then four-replica GaMD trajectories are joined into a single MR-GaMD trajectory to collect significant information with regard to conformational alterations of K-Ras. A program PyReweighting[84] proposed by Miao et al. is utilized to accurately reweight MR-GaMD simulations and recognize the original free energy of the studied systems. As for the current cMD and GaMD simulations, all chemical bonds connecting to hydrogen atoms are constrained by means of the SHAKE algorithm.[85] The Langevin dynamics[86] with a collision frequency of 2.0 ps^{-1} is carried out to regulate the temperature of six simulated systems. The particle mesh Ewald (PME) method[87] with an appropriate cutoff value of 10 Å is employed to estimate electrostatic interactions, and this cutoff is also applied to treat the van der Waals interactions. All current simulations are executed by using the program pmemd.cuda inlayed in Amber 18.[88,89]

Essential Dynamics (ED) Analysis. Essential dynamics (ED) analysis,[61] also termed as principal component analysis, is thought to be an efficient approach to probe collected motions of protein domains. This method has been extensively utilized to filter large concerted motions from an ensemble of structures stemming from the experiment or molecular simulations. In this work, ED analysis can be achieved by following the following three steps: (1) a covariance matrix is constructed by using the atomic coordinates of the C_α atoms of K-Ras kept in the single joined MR-GaMD trajectory, (2) the covariance matrix is diagonalized to yield the eigenvalues and eigenvectors, in which the eigenvalues reflect the total motion

https://doi.org/10.1021/acs.jcim.0c01470
J. Chem. Inf. Model. 2021, 61, 1954−1969

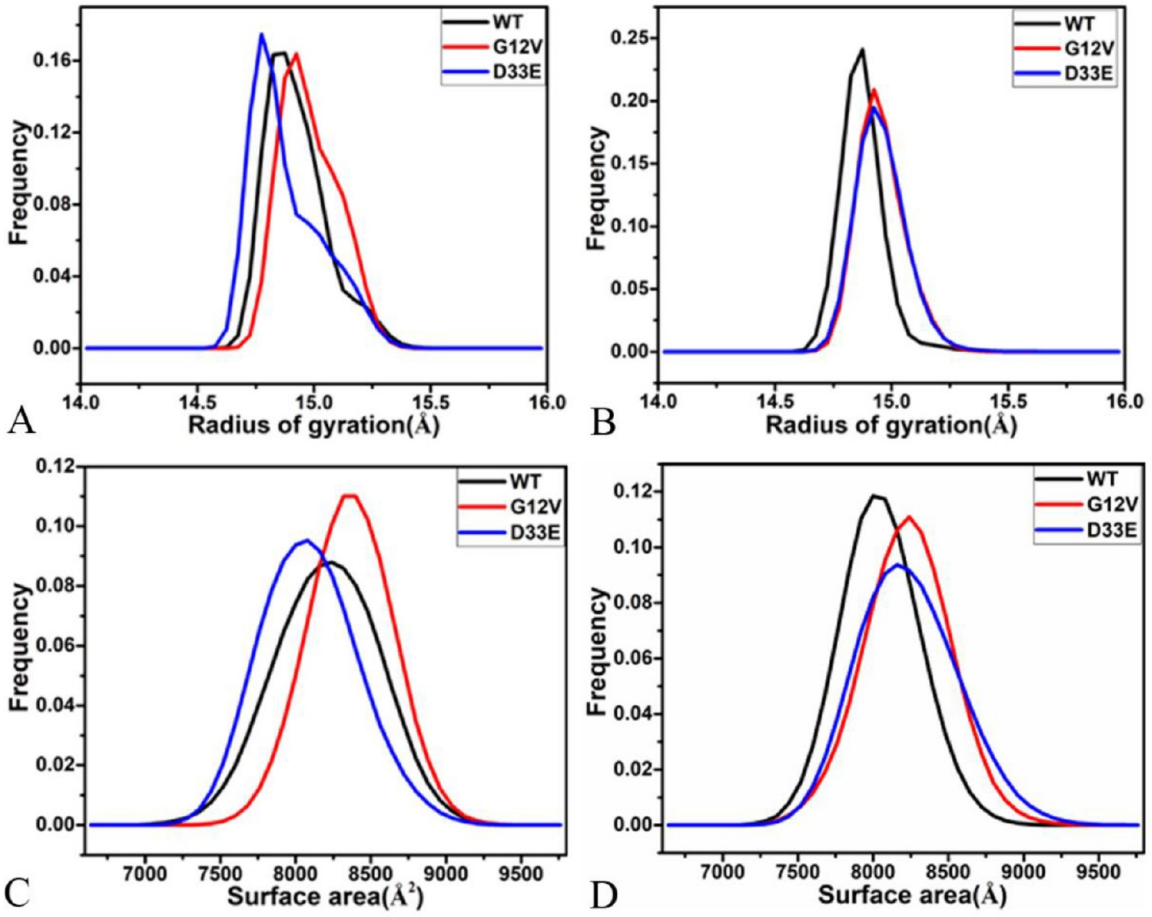

Figure 2. Radius of gyrations and molecular surface areas: (A) gyrations of the GDP-bound WT and mutated K-Ras, (B) gyrations of the GTP-associated WT and mutated K-Ras, (C) molecular surface areas of the GDP-bound WT and mutated K-Ras, and (D) molecular surface areas of the GTP-complexed WT and mutated K-Ras.

strength and the eigenvectors characterize the motion directions of domains of K-Ras along a conformational subspaces, (3) the first eigenvector is visualized to depict motion behavior of domains by means of the initialized structure. With respect to the ED analysis, the eigenvectors with the larger eigenvalues are responsible for the overall concerted motions of domains in K-Ras. The ED analysis is conducted on the single joined MR-GaMD trajectory by utilizing the program CPPTRAJ[90] in Amber18. To obtain the visualization of the results from our ED analysis, the software VMD[91] and PyMOL (www.pymol.org.) are used to analyze the single joined MR-GaMD trajectory, depict pictures, and reveal the mutation-mediated effect on the conformational changes of K-Ras.

Dynamics Cross-Correlation Maps. Dynamics cross-correlation maps (DCCMs)[92−94] play significant roles in insights into internal dynamics of proteins and motion modes between residues in proteins. The matrix elements C_{ij} of DCCMs are determined using the following equations

$$C_{ij} = \frac{\langle \Delta r_i \cdot \Delta r_j \rangle}{(\langle \Delta r_i^2 \rangle \langle \Delta r_j^2 \rangle)^{1/2}} \quad (7)$$

in which Δr_i denotes the displacement of the ith C_α atom deviating from its averaged position and the angle bracket indicates an ensemble average over the conformations saved in the single joined MR-GaMD trajectory. The values of C_{ij} fluctuate from −1 to +1, of which the positive and negative C_{ij} individually reflect the positively correlated motions and anticorrelated movements between residues. Through the changes of C_{ij}, the mutation-mediated influences on internal dynamics of the GTP- and GDP-bound K-Ras can be efficiently evaluated. In this study, the calculations of DCCMs are implemented by means of the program CPPTRAJ inlayed in Amber 18.[90] The extent of the correlated motions between residues of K-Ras is visually exhibited by using the color-coded styles.

RESULTS AND DISCUSSION

Changes of Structural Flexibility Induced by G12V and D33E. To unveil mutation-induced impacts on the total structural flexibility of K-Ras, gyrations and molecular surface areas (MSAs) of the GDP/GTP-bound WT and mutated K-Ras are calculated by utilizing the single joined MR-GaMD trajectory (Figure 2). Compared to the GDP-bound WT K-Ras, the gyration of the GDP-bound G12V K-Ras is increased by ∼0.12 Å, while that of the GDP-bound D33E K-Ras is decreased by ∼0.10 Å (Figure 2A). The gyrations of the GTP-associated G12V and D33E K-Ras are enhanced by ∼0.10 Å by comparison with the WT one (Figure 2B). By comparison with the GDP-associated WT K-Ras, the MSA of the G12V K-Ras is raised by ∼160 Å^2 but that of the D33E K-Ras is reduced by ∼160 Å^2 (Figure 2C). Compared to the GTP-associated WT K-Ras, mutations G12V and D33E individually result in the

https://doi.org/10.1021/acs.jcim.0c01470
J. Chem. Inf. Model. 2021, 61, 1954−1969

increases of 160 and 240 Å^2 in the MSAs of the GTP-bound K-Ras (Figure 2D). Consequently, G12V and D33E generate different effects on the total structural flexibility of the GDP/GTP-associated K-Ras. Briefly, the G12V induces a structural expansion of the GDP-bound K-Ras while D33E causes a structural reduction of the GDP-complexed K-Ras; however, two mutations G12V and D33E strengthen the total structural flexibility of the GTP-associated K-Ras. Hence, oncogenic G12V and D33E mutations lead to possible alteration of the nucleotide-binding sites, which certainly affects binding of GNEFs or effectors to K-Ras.[73,95]

To further understand the changes in the flexibility of the GDP/GTP-complexed K-Ras induced by mutations, the difference in root-mean-square fluctuations (RMSFs) of the C_α atoms are calculated using the equation $\Delta RMSF = RMSF_{mutant} - RMSF_{WT}$ (Figure 3). By referencing the GDP-bound WT K-Ras, G12V obviously strengthens the structural flexibility of SW1, and D33E enhances the structural flexibility of the most regions in SW1 but weakens that of the region near the residue 40 (Figure 3A). Compared to the GDP-bound WT K-Ras, G12V evidently raises the structural flexibility of SW2, but D33E highly reduces that of SW2 in K-Ras (Figure 3A). By comparison with the GTP-complexed WT K-Ras, the structural flexibility of SW1 is highly strengthened by G12V and D33E, meanwhile the flexibility of SW2 is also evidently increased by D33E, although that of the most regions in SW2 is enhanced by G12V, that of the region near the residue A59 in SW2 is weakened due to G12V (Figure 3B). Compared to the GDP/GTP-bound WT K-Ras, G12V slightly heightens the structural flexibility of the helix α_3, but D33E softly weakens that of this helix. In addition, the flexibility of the N-terminal in the GTP-bound K-Ras is heavily affected by G12V and D33E compared to that in the GDP-associated K-Ras, which is attributed to a more charge of GTP relative to GDP. It is well-known that SW1 is involved in binding domains of GNEFs or effectors, and thus, the changes in the structural flexibility of SW1 caused by mutations heavily affect binding of GNEFs or effectors to K-Ras and regulate the activity of oncogenic K-Ras, which is also revealed by the previous works.[72,96] Besides this, the altered flexibility of SW2 exerts a vital effect on binding and activation of effectors by disturbing dynamic interactions involving residues outside the effector binding region.[97,98]

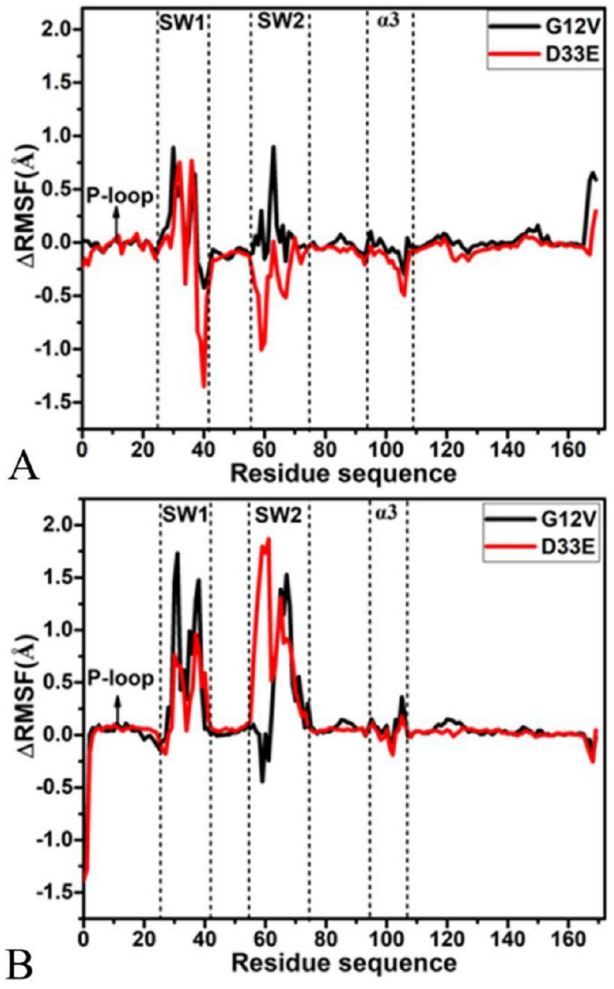

Figure 3. Difference of root-mean-square fluctuations (RMSFs) of C_α atoms induced by G12V and D33E: (A) the GDP-bound K-Ras and (B) the GTP-associated K-Ras.

A magnesium ion Mg^{2+} appears in the crystal structures of the GDP/GTP-complexed K-Ras (Figure 1, parts A and B), and its stability during MR-GaMD simulations is significant for the understanding of the function of K-Ras. Thus, the distances of Mg^{2+} away from the oxygen atoms O2B and O2G of GTP and O1B and O3B of GDP are estimated and their frequency distribution are depicted in the Supporting Information Figure S1. Parts A and B of Figure S1 suggest that Mg^{2+} is highly stable through the entire MR-GaMD simulation, and two mutations hardly generate influences on the stability of Mg^{2+} in the GTP-bound K-Ras, which functionally facilitates the hydrolysis of GTP into GDP.[20,76] Although mutations G12V and D33E do not also obviously affect the distance of Mg^{2+} away from the oxygen atom O3B of GDP, D33E increases the distance between Mg^{2+} and the oxygen atom O1B of GDP (Figure S2, parts C and D). Thus, the stability of Mg^{2+} in the GDP-bound D33E K-Ras is weaker than that in the GTP-bound D33E K-Ras, which is not observed and clarified in the previous works. This result suggests that D33E yields significant influence on the conformational transformation of the switch domain in the GDP-bound K-Ras and changes the activity of K-Ras in inactive state.[96]

Mutation-Mediated Effect on Internal Dynamics of the GDP-/GTP-Bound K-Ras. To explore mutation-induced effect on conformational alterations of K-Ras, DCCMs are estimated by wielding the coordinates of the C_α atoms (Figure S2). It is observed that motion modes between residues of the GDP-bound WT K-Ras are similar to that of the GTP-associated one (Figure S2, parts A and B). In the GDP/GTP-bound WT K-Ras, the regions R1, R2, and R3 respectively characterize the strongly anticorrelated motions of SW1 relative to the P-loop, SW2 relative to SW1, and the helix α_3 relative to SW1 (Figures 1A and S2, parts A and B). The region R4 in the WT K-Ras yields the strongly positive correlated motions of the loop linking with SW2 relative to the P-loop, moreover this motion in the GTP-bound WT K-Ras is slightly stronger than that in the GDP-bound one (Figures S2A and S2B).

Compared to the GDP- and GTP-associated WT K-Ras, G12V weakens the anticorrelated motions occurring in the regions R1, R2, and R3 (Figure S2, parts C and D); although G12V hardly exerts the obvious influence on the positively correlated motions of the region R4 in the GDP-bound G12V K-Ras, it evidently weakens that of this region in the GTP-associated G12V K-Ras (Figure S2, parts C and D). By

https://doi.org/10.1021/acs.jcim.0c01470
J. Chem. Inf. Model. 2021, 61, 1954−1969

referencing the GDP-bound WT K-Ras, D33E only slightly abates the anticorrelated motions of the regions R2 and R3, but it obviously enhances the positively correlated motions of the region R4 (Figure S2E). By comparison with the GTP-bound WT K-Ras, D33E greatly weakens not only the anticorrelated motions in the regions R1-R3 but also the positively correlated movement of the region R4 (Figure S2F). Hence two mutations change motion modes between SW1 and P-loop as well as between SW2 and SW1, which in turn tunes the activity of K-Ras and affects bindings of GNEFs or effectors to K-Ras.[23,99] The changes in motion modes of the helix α_3 relative to SW1 and P-loop induced by mutations have been reported to function as an allosteric site regulation on the conformational order of SW2.[71,100]

With the aim of further probing mutation-mediated impacts on dynamics behavior of K-Ras, ED analysis is carried out by diagonalizing a covariance matrix constructed with the coordinates of the C_α atoms. The function of eigenvalues VS eigenvectors arising from ED analysis (Figure S3) suggests that G12V and D33E greatly strengthen the total motion strength of the GDP/GTP-bound K-Ras. Besides this, the first eigenvector stemming from ED analysis is visually exhibited in Figure 4, and the results indicate that two switch domains, SW1 and SW2, possess the most flexible motion behavior.

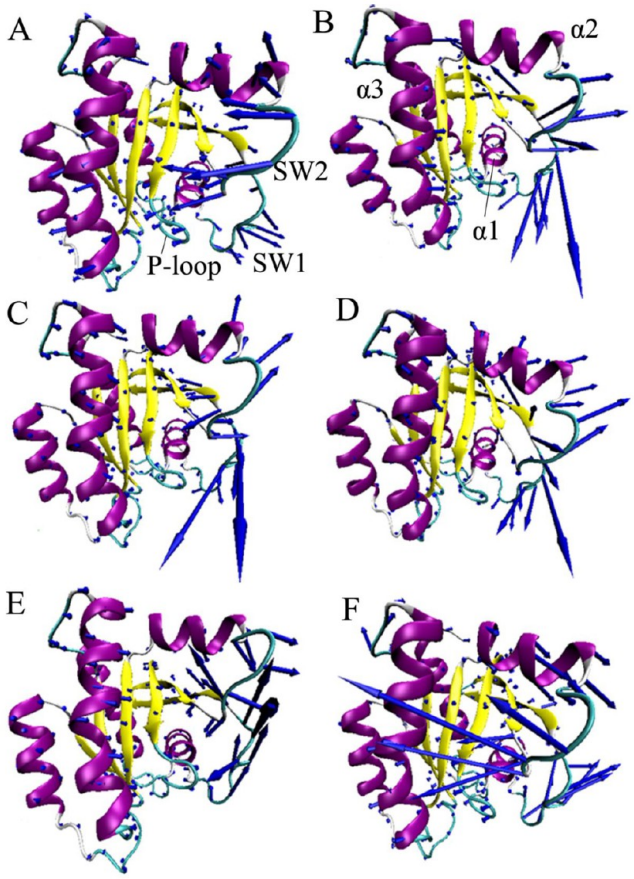

Figure 4. Collective motions of the domains in K-Ras along the first eigenvector arising from essential dynamics analysis: (A) the GDP-bound WT K-Ras, (B) the GTP-bound WT K-Ras, (C) the GDP-associated G12V K-Ras, (D) the GTP-associated G12V K-Ras, (E) the GDP-complexed D33E K-Ras, and (F) the GTP-complexed D33E K-Ras. In this figure, the direction and length of arrows separately describe the motion direction and strength of domains in K-Ras.

Compared to the GDP-associated WT K-Ras (Figure 4A), G12V not only changes the motion direction of SW1 but also strengthens the motion strength of SW1; meanwhile, G12V also alters the motion direction of SW2 but hardly inhibits the motion strength of SW2 (Figure 4C). By referencing the GTP-complexed WT K-Ras (Figure 4B), G12V weakens the motion of SW1, but it strengthens the movement of the helix α_2 in SW2 (Figure 4D). By comparison with the GDP-associated WT K-Ras (Figure 4A), D33E not only evidently changes the movement direction of SW1 and SW2 but also enhances the motion strength of SW1 (Figure 4E) Compared to the GTP-associated WT K-Ras (Figure 4B), D33E extremely alters the movement direction of SW1 and SW2, and in the meantime, D33E exceedingly strengthens the movement of SW2 but slightly weakens the motion of SW1. Our current work explicitly displays that G12V and D33E change the motion tendency and intensity between SW1 and SW2, which is not revealed by the previous works. The alterations in dynamics behavior of SW1 and SW2 induced by G12V and D33E lead to the changes in the conformational flexibility of SW1 and SW2,[20,72,75] biochemical difference of K-Ras,[28] and the tuning on the active site conformation when Ras is in associations with effector proteins.[6,101] Moreover, the adjustment of the mutation in the P-loop on the activity of K-Ras has been applied to rationally direct design of the SW2 covalent binders.[102]

Conformational Changes of K-Ras Probed by Free Energy Landscapes. Free energy profiles are of significance for understanding influences of G12V and D33E on conformational alterations of the GDP/GTP-bound K-Ras. Therefore, free energy landscapes are constructed by using the distance of the residue T35 in the SW1 away from the residue E62 in the SW2 and root-mean-square (RMSDs) of backbone atoms as reaction coordinates (Figures 5−7). The distance of T35 away from E62 can efficiently reflect the conformational state transformation between SW1 and SW2, while RMSDs can rationally embody total structural fluctuations of K-Ras, which is the reason we select them as reaction coordinates.

As for the GDP-bound WT K-Ras, MR-GaMD simulations detect three free energy basins I, II, and III, and their potential well depths are 8.2, 10.0, and 8.2 kcal/mol (Figure 5A). Three representative structures I, II, and III, are superimposed with the crystal structure of the GDP-bound WT K-Ras (Figure 5B), and the results not only suggest that the structure I is very close to the crystal structure but also show that the conformations of two switches SW1 and SW2 are highly disordered. The distances between SW1 and SW2 in the structures I, II and III are 11.9, 27.4, and 17.2 Å separately (Figures S4A-4C), indicating that the conformations between SW1 and SW2 separately exhibit the closed, open, and semiclosed states in the GDP-bound WT K-Ras. Furthermore, the distance between SW1 and SW2 in structure I is also close to the distance of 11.3 Å in the crystal structure of the GDP-associated WT K-Ras (Figure 1A). Although the conformations of SW1 and SW2 are highly disordered, other regions of K-Ras, GDP, and magnesium ion (Mg^{2+}) are greatly stabilized during MR-GaMD simulations (Figures 5B and S4D). Figure 5C shows that the GTP-associated WT K-Ras also possesses three states, I, II, and III, individually situated at the potential wells of 8.8, 10.0, and 10.0 kcal/mol. The distances of SW1 away from SW2 are 10.3, 22.5, and 17.5 Å in the structures I, II, and III of the GTP-associated WT K-Ras, which respectively imply the closed, open, and semiclosed states

https://doi.org/10.1021/acs.jcim.0c01470
J. Chem. Inf. Model. 2021, 61, 1954−1969

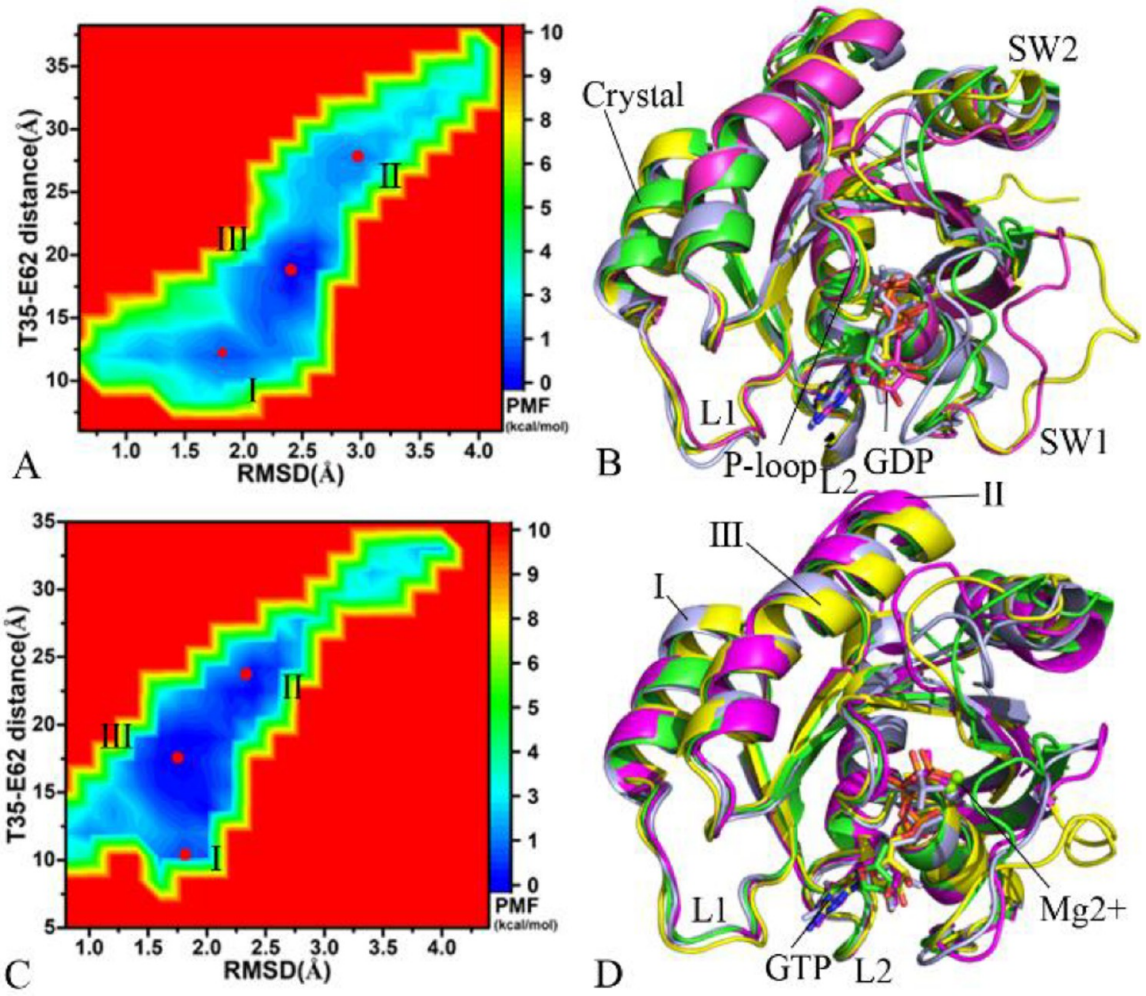

Figure 5. Free energy landscapes and superimpositions of representative structures: (A) free energy landscapes of the GDP-bound WT K-Ras, (B) alignment of three representative structures of the GDP-bound WT K-Ras falling into the energy basins I, II, and III with the crystal structure, (C) free energy landscapes of the GTP-associated WT K-Ras, and (D) superimposition of three representative structures of the GTP-associated WT K-Ras sited at the energy basins I, II, and III with the crystal structure. K-Ras, GDP/GTP, and magnesium ions are displayed by using cartoon, stick, and ball modes.

between SW1 and SW2 (Figure S5A−C). The superimposition of K-Ras, GTP, and magnesium ion (Mg^{2+}) in the structures I, II, and III with that in the crystal structure indicates that although the conformations of SW1 and SW2 in the GTP-associated WT K-Ras are highly unordered, they hardly affect the stability of GTP and Mg^{2+} (Figures 5D and S5D). Therefore, it is concluded that the conformations of SW1 and SW2 in the GDP/GTP-complexed K-RAs can realize interconversion between the closed and open states. Because the well depth of states I and II in the GTP-bound WT K-Ras is smaller than those in the GDP-bound WT K-Ras, the transformation possibility between the closed and open states of SW1 and SW2 in the GTP-complexed WT K-Ras is higher than that in the GDP-associated WT K-Ras. Structurally, the negative charges of GTP is more than that of GDP; thus, GTP yields stronger long-range electrostatic interactions with those residues with positive and negative charges, which possibly leads to a shallower potential well in the GTP-bound WT K-Ras. Consequently, the GTP-bound WT K-Ras is easier to adopt an active conformational state than the GDP-associated WT K-Ras,[71] which quantitatively evaluates structural and dynamical features of active and inactive states and conformational interconversion in the GDP/GTP-bound K-Ras.[75] The above analyses are also compatible with the existence of multiple switch conformations within each nucleotide state.[23,103,104]

Compared to the GDP-bound WT K-Ras, G12V induces four different energy states (Ia, Ib, IIa, and IIb) located at the potential well of 10.0 kcal/mol (Figure 6A), and the information not only shows the conformational diversity of the GDP-associated G12V K-Ras but also verifies the high flexibility and disorder of the switch domains (Figure 6B). The distance of SW1 away from SW2 in the structures Ia, Ib, IIa, and IIb are respectively 12.2, 14.8, 22.4, and 24.4 Å in the GDP-bound G12V K-Ras (Figures S6A-S6D); thus, the structures Ia and Ib exhibit a closed state between SW1 and SW2, while the conformations IIa and IIb show an open conformation. Similar to the GDP-bound WT K-Ras, G12V hardly affects the stability of GDP, Mg^{2+}, and the nonswitch domains of K-Ras (Figures 6B and S6E). Different from the GDP-bound WT K-Ras, G12V leads to the direct transformation between the closed and open states between SW1 and SW2 and does not induces the appearance of a semiclosed state. By comparison with the GTP-bound WT K-Ras, G12V

https://doi.org/10.1021/acs.jcim.0c01470
J. Chem. Inf. Model. 2021, 61, 1954−1969

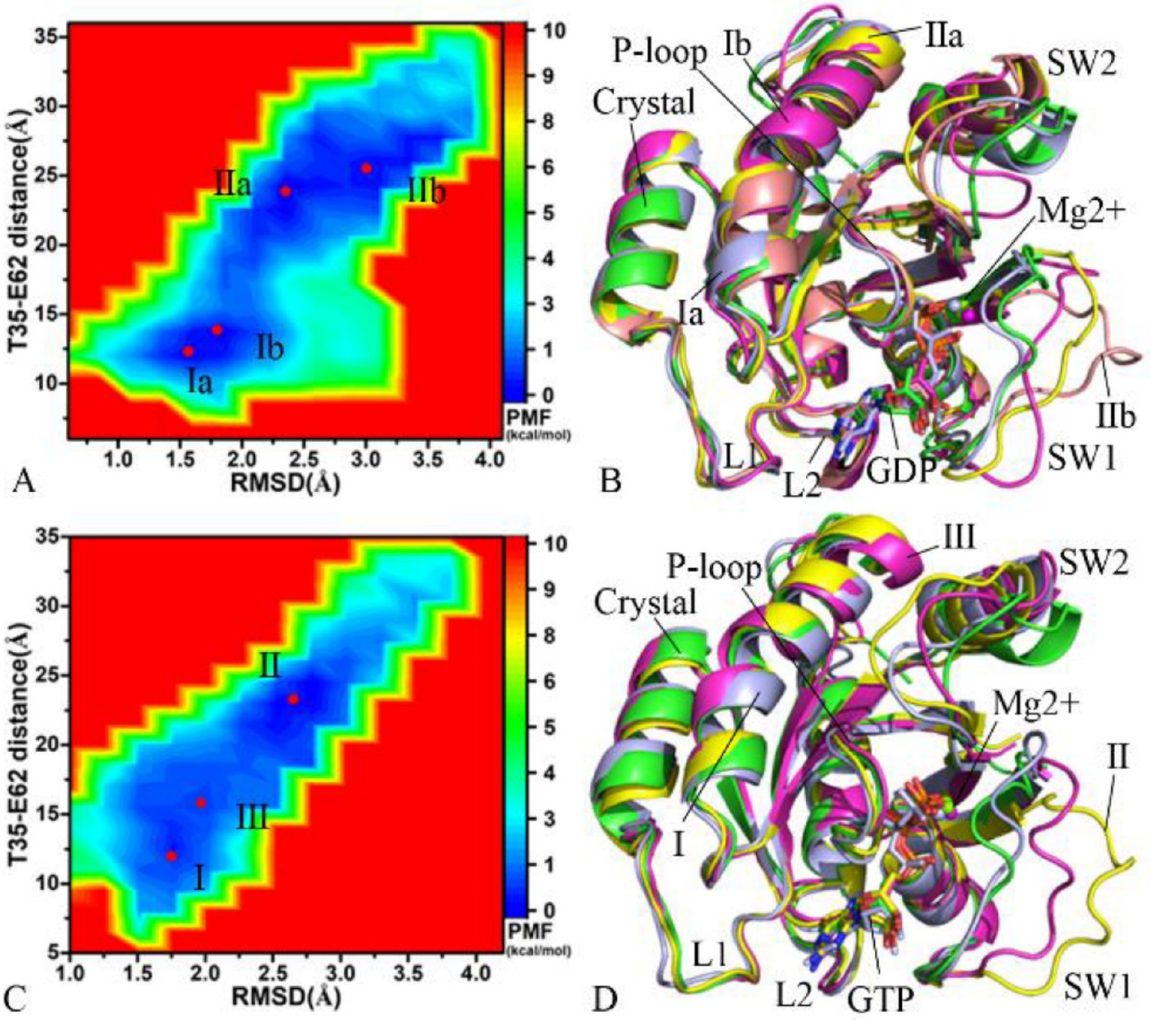

Figure 6. Free energy profiles and alignments of representative structures: (A) free energy landscapes of the GDP-associated G12V K-Ras, (B) comparisons of four representative structures of the GDP-bound G12V K-Ras located at the energy basins Ia, Ib, IIa, and IIb with the crystal structure, (C) free energy landscapes of the GTP-complexed G12V K-Ras and (D) superimposition of three representative structures of the GTP-associated G12V K-Ras corresponding to the energy basins I, II, and III with the crystal structure. K-Ras, GDP/GTP, and magnesium ions are exhibited in cartoon, stick, and ball styles.

also induces three free energy states, I, II, and III (Figure 6C), but the conformational states I and II are located at deeper potential wells and the conformational state III at a shallower potential well (Figure 6C). The distance between SW1 and SW2 in the structures I, II, and III are independently 12.1, 23.1, and 16.6 Å in the GTP-complexed G12V K-Ras (Figures S7A−C), which individually displays the close, open and semiclosed states. Similar to the GTP-associated WT K-Ras, although two switch domains SW1 and SW2 are greatly out-of-order in the G12V K-Ras (Figure 6D), G12V scarcely affects the stability of GTP and Mg^{2+} (Figure 6D and S7D). It is worth noting that the loop of SW1 is completely extend and away from the P-loop in the G12V mutated state (Figures 5D and 6D), which significantly disturbs binding of GNEFs or effectors and potentially tunes the activity of oncogenic K-Ras.[105] A study from atomistic molecular simulations and Markov state modeling confirms that G12 mutations modify K-Ras dynamics and tune the activity of K-Ras.[70] The work of Buhrman et al. also suggests that mutations G12V and Q61L induce the "on" and "off" conformations of the allosteric switch in the GTP-bound K-Ras,[106] but this does not explicitly display the appearance of a semiclosed or an intermediary state.

By comparison with the GDP-bound WT K-Ras, D33E leads to the appearance of two states I and II situated at the potential well of 10.0 and 7.6 kcal/mol and induces a conformational convergence (Figure 7A). The distances between SW1 and SW2 in the structures I and II are individually 10.1 and 25.9 Å (Figure S8, parts A and B), separately implying that they are the closed and open states of the switch domains in the GDP-associated D33E K-Ras. Similar to the GDP-bound WT K-Ras, although D33E results in the big conformational changes of the switch domains, it hardly exerts an effect on the stability of GDP and Mg^{2+} (Figures 7B and S8C). In comparison with the GDP-complexed WT K-Ras, D33E makes the depth of the potential well II shallower than that in the WT K-Ras; hence, the switch domains of the GDP-bound D33E K-Ras mainly exist in the closed formation. Compared to the GTP-coupled WT K-Ras, D33E also causes three energetic states I, II, and III individually falling into the potential well of 7.8, 10.0, and 10.0 kcal/mol, but the depth of the potential well in state I is shallower than that of the WT K-Ras (Figure 7C). It is

https://doi.org/10.1021/acs.jcim.0c01470
J. Chem. Inf. Model. 2021, 61, 1954−1969

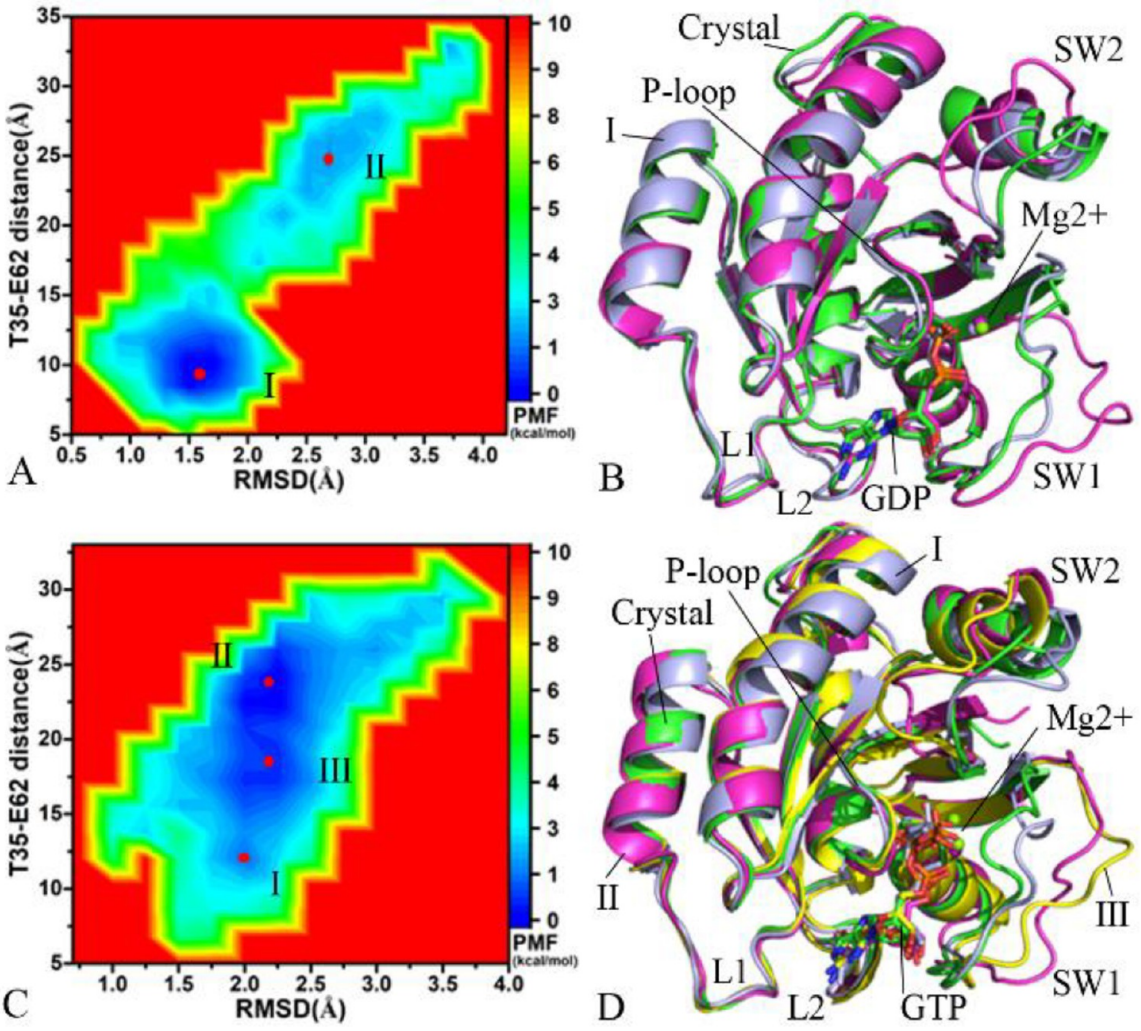

Figure 7. Free energy landscapes and superimpositions of representative structures: (A) free energy landscapes of the GDP-complexed D33E K-Ras, (B) alignments of two representative structures of the GDP-associated D33E K-Ras falling into energy basins I and II with the crystal structure, (C) free energy landscapes of the GTP-bound D33E K-Ras and (D) superimposition of three representative structures of the GTP-complexed D33E K-Ras corresponding to energy basins I, II, and III with the crystal structure. K-Ras, GDP/GTP, and magnesium ions are shown with cartoon, stick, and ball modes.

separately 12.4, 22.6, and 17.9 Å from SW1 to SW2 in the structures I, II, and III of the GTP-combined D33E K-Ras, which displays the closed, open, and semiclosed states, respectively (Figures S9A−C). Despite high disorder of the switch domains (Figure 7D), D33E scarcely hardly interferes with the stability of GTP, Mg^{2+}, and the nonswitch domains of K-Ras (Figure S9D). In comparison to the GTP-complexed WT K-Ras, although D33E does not change the energetic states, the conformations of the switch domain are more populated at the open state in the GTP-bound D33E K-Ras (Figures 5C and 7C). The X-ray crystal structure of the rare GDP-bound D33E tumorigenic K-Ras determined by Lu et al. uncovers that D33E not only induces an open SW1 state but also alters the SW2 conformation, and their results also show an impaired interaction with the guanine exchange factor SOS and loss of the GAP-dependent GTPase activity.[96]

Based on the aforementioned analyses, three conclusions are drawn as below: (1) the closed and open states of SW1 and SW2 in the GDP/GTP-coupled K-Ras are interchangeable, but G12V and D33E generate more apparent influences on free energy profiles of the GDP-associated inactive K-Ras than that of the GTP-complexed active one, (2) G12V and D33E produce different effect on the depth of potential well in the various states, which potentially tunes the activity of K-Ras, and (3) high disorder of the switch domains in the GDP/GTP-bound K-Ras hardly affects the stability of GDP, GTP, Mg^{2+}, and the nonswitch domains of K-Ras. The changes in the conformational disorder of SW1 and SW2 caused by G12V and D33E can be potentially applied to tune the activity of K-Ras. In fact, a significant mutation G13D has possessed unique features that destabilize the nucleotide-binding pocket[28] and shown rapid nucleotide exchange kinetics compared with other mutants.[40] The previous works anchoring to a lipid bilayer suggest that membranes with high electrostatic environments help to tune the activity of K-Ras,[33,34,36] which also points out a future direction toward K-Ras.

Interaction Networks of GDP and GTP with K-Ras Affected by Mutations. To check influences of G12V and D33E on bindings of GDP and GTP to K-Ras, a protein−ligand interaction profiler (PLIP) server[107] is applied to detect interaction networks of GDP and GTP with K-Ras in the closed and open states (Figure 8). The frequency distribution

https://doi.org/10.1021/acs.jcim.0c01470
J. Chem. Inf. Model. 2021, 61, 1954−1969

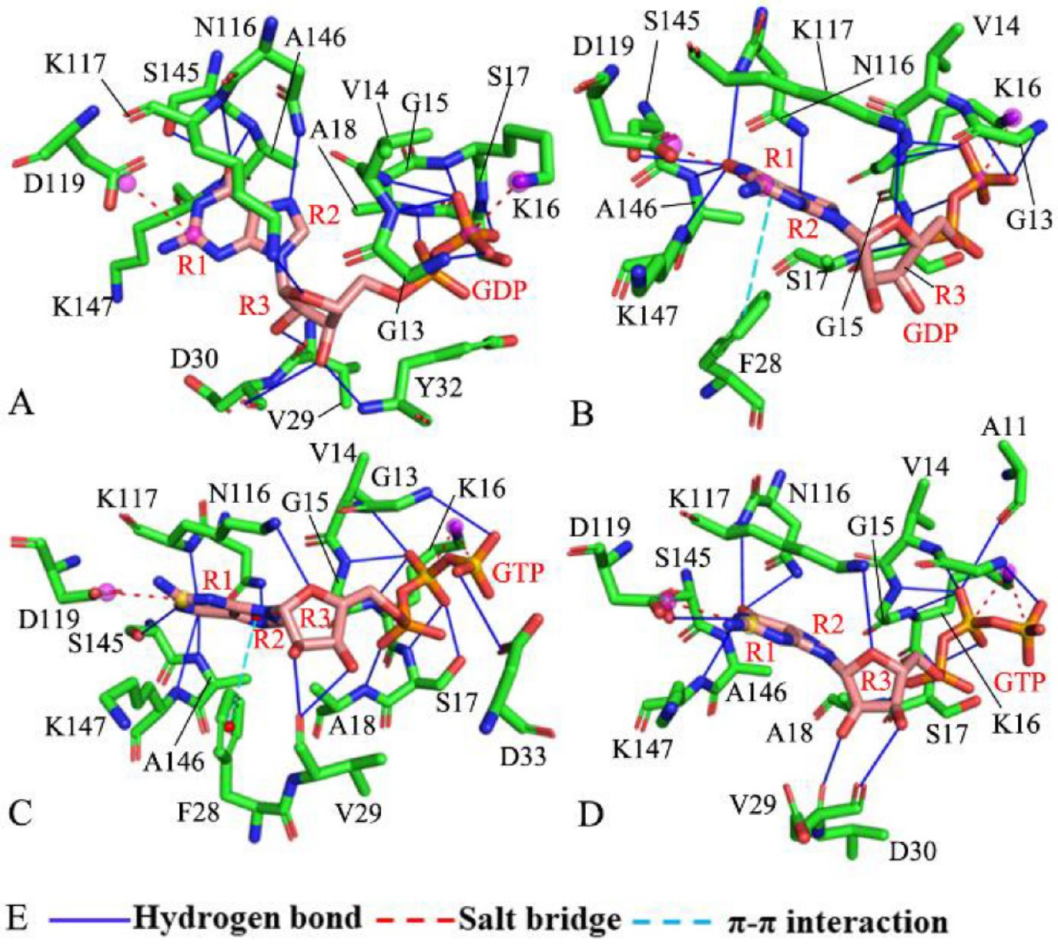

Figure 8. Interaction networks of GDP and GTP with K-Ras in the closed and open states: (A and B) separately corresponding to the GDP-residue interactions in the closed and open states of the GDP-bound WT K-Ras, (C and D) individually corresponding to the GTP-residue interactions in the closed and open states of the GTP-associated WT K-Ras, and (E) interaction types.

of distances involved in key interactions are also computed by using the single joined MR-GaMD trajectory (Figures 9 and 10). Meanwhile hydrogen-bonding interactions (HBIs) of GDP and GTP with K-Ras are also analyzed by utilizing the CPPTRAJ module in Amber and the results are provided in Tables 1 and 2.

For the closed and open states of the GDP-associated WT K-Ras, the NH groups of backbones from the residues G13, V14, G15, K16, S17, and A18 yield HBIs with the phosphate group of GDP (Figure 8, parts A and B). Except for V14, the occupancy of HBIs between GDP and the residues G15, K16, S17, and A18 is higher than 72.3% (Table 1). The residues N116, K117, S145, A146, and K147 in the WT K-Ras form HBIs with the guanine group (the rings R1 and R2) of GDP in two states (Figure 8, parts A and B) and their occupancy is higher than 61.9% excluding the residues K117 (Table 1). In addition, the residues V29, D30, and Y32 also yield HBIs with the ring R3 of GDP (Figure 8, parts A and B) and their occupancy ranges from 29.8% to 41.4% (Table 1), consequently the stability of these HBIs during MR-GaMD simulations are weaker than that of HBIs with the phosphate and guanine groups of GDP. The cause leading to this result may be attributed to high disorders of SW1 and SW2 revealed by the previous FELs. A favorable $\pi-\pi$ interaction[108] is produced between the phenyl group of F28 and the guanine group of GDP in the open state of the GDP-bound WT K-Ras (Figure 8B) and its distance frequency is locate at ∼5.1 Å (Figure 9A), but this favorable interaction disappears in the closed state (Figure 8A). Two salt bridge interactions appear in the closed and open states of the GDP-bound K-Ras, one is formed between the carbonyl of D119 and the guanine group of GDP, another stems from the positive charge group of K16 and the phosphate group of GDP (Figure 8, parts A and B). The distances of the salt bridge interactions of K16 and D119 with GDP are separately distributed at ∼3.39 and 3.63 Å (Figure 10, parts A and B). Compared to the GDP-bound WT K-Ras, the changes in the occupancy of HBIs of the residues G13, V14, G15, K16, S17, and A18 with the phosphate of GDP induced by G12V and D33E ranges from 0 to 2.9% (Table 1), verifying that G12V and D33E hardly exert an effect on the stability of these HBIs. Furthermore the residues G13, V14, G15, K16, S17, and A18 are situated at the P-loop (Figure 10C), which rationally explains the high order of the P-loop conformations unveiled by the previous FELs in the WT and mutated K-Ras. Similarly, G12V and D33E also scarcely produce obvious influences on the occupancy of the HBIs of the guanine group from GDP with the residues N116, K117, S145, A146, and K147 located at the loops L1 and L2 (Table 1 and Figure 10C), which provides favorable forces for the conformational orders of the loops L1 and L2 in the GDP-associated K-Ras. However, the HBIs of V29, D30, and Y32 with GDP is greatly disturbed by G12V and D33E; thus, these

https://doi.org/10.1021/acs.jcim.0c01470
J. Chem. Inf. Model. 2021, 61, 1954−1969

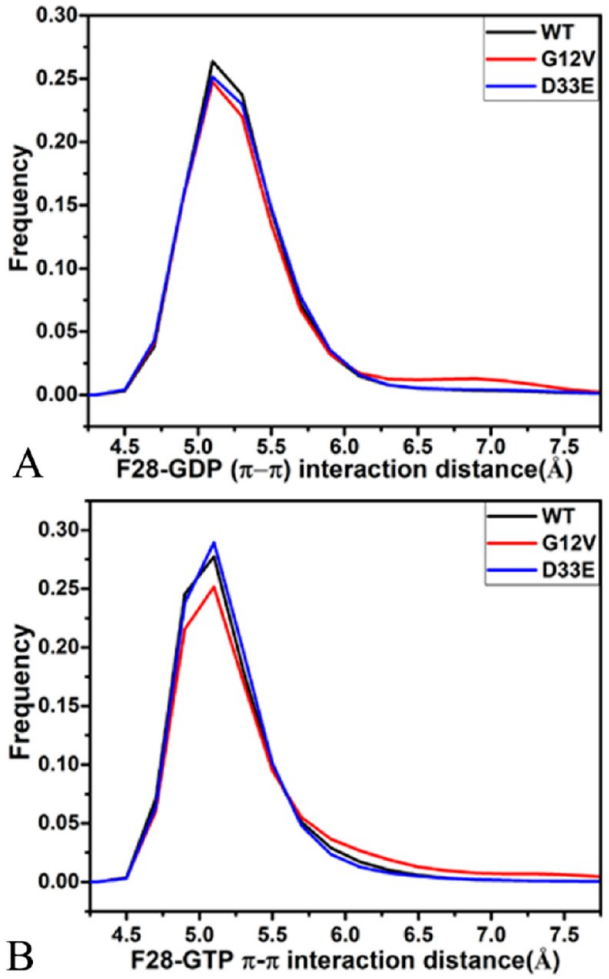

Figure 9. Π−π interactions of the residue F28 with GDP and GTP: (A) the GDP-bound WT and mutated K-Ras and (B) the GTP-associated WT and mutated K-Ras.

two mutations highly affect the structural flexibility of SW1 and SW2, which shows good consistency with the previous analyses of RMSFs and DCCMs. The $\pi-\pi$ interaction of F28 and salt bridge interactions of K16 and D119 with GDP are hardly affected, which further enhances the conformational orders of P-loop and L1 (Figures 9A and 10A−C).

With regard to the closed and open formation of the GTP-bound WT K-Ras, the phosphate group of GTP produces the HBIs with the NH group of backbones in the residues G13, V14, G15, K16, S17, and A18 (Figure 8, parts C and D). Except for V14, the occupancy of the HBIs between other residues and GTP exceeds 85.8% (Table 2). The guanine group of GTP is involved in the HBIs with the residues N116, K117, S145, A146, and K147 in the WT K-Ras (Figure 8, parts C and D) and their occupancy is higher than 64.2% apart from K117 (Table 2), indicating that these HBIs are highly stable through MR-GaMD simulations. Besides, the residues V29 and D30 also generate the HBIs with the ring R3 of GTP (Figures 8, parts C and D), but according to their occupancy, which is lower than 36.2% (Table 2), the stability of these HBIs is weaker than that of HBIs with the phosphate and guanine groups of GTP. The phenyl group of F28 forms the favorable $\pi-\pi$ interaction with the guanine group of GTP in the closed state of the GTP-bound WT K-Ras and its distance frequency is situated at ∼5.1 Å (Figure 9B), however this interaction disappears in the open state of the GTP-associated WT K-Ras (Figure 8D). GTP also yields three salt bridge interactions with residues D119 and K16, in which the carbonyl group of D119 generates a salt bridge with the guanine group of GTP while the positive charge group of K16 forms two salt bridges with the PB and PG groups in the phosphate of GTP (Figure 8, parts C and D). The frequency distributions of three salt bridge-dependent distances are located at 3.63, 3.39, and 3.75 Å for the D119-guanine, K16-PB, and K16-PG in the GTP-bound WT K-Ras, respectively (Figure 10D−F). By comparison with the GTP-associated WT K-Ras, the changes in the occupancy of HBIs of the residues G13, V14, G15, K16, S17, and A18 with the phosphate of GTP caused by G12V and D33E are lower than 3.7% (Table 2), showing that G12V and D33E scarcely affect the stability of the GTP/K-Ras HBIs relating with the P-loop. Thus these HBIs maintain the high order of the P-loop conformations in the GTP/K-Ras complexes. On the other hand, the changed occupancy of the HBIs between GTP and two loops L1 and L2 induced by G12V and D33E is lower than 6.4% (Table 2), which is partially responsible for high order of L1 and L2 revealed by the previous FELs. However, two HBIs with residues V29 and D30 situated at the SW1 change evidently (Table 2), which rationally explains the disorder of the SW1 in the GTP-associated K-Ras. By referencing the GTP-bound WT K-Ras, G12V and D33E hardly produce impacts on the salt bridge interaction between the carbonyl of D119 and the guanine group of GTP, which further preserves the order of the loop L1 (Figure 10, parts C and D). Intriguingly, D33E scarcely alters two salt bridge interactions of the positive charge group of K16 with the phosphate group of GTP. Although G12V weakens the salt bridge between K16 and the PB group in the phosphate of GTP, it strengthens the salt bridge interaction of K16 with the PG group of the phosphate of GTP (Figure 10, parts E and F).

In summary, G12V and D33E bring different influences on interaction networks of GDP and GTP with K-Ras: (1) G12V and D33E hardly affect the HBIs of the loops L1, L2, and P-loop with GDP and GTP, which highly maintains the conformational order of these several loops in the WT and mutated K-Ras, (2) G12V and D33E heavily disturb the HBI network of SW1 with GTP and GDP, which rationally explains the reason the conformations of SW1 and SW2 are exceedingly disordered in the WT and mutated states of K-Ras revealed by the previous FELs, and (3) although G12V and D33E scarcely affect the salt bridge interactions of D119 and K16 separately with the guanine group and the PB group of GDP and GTP, G12V obviously changes the interaction strength of the salt bridge between K16 and the PG group of GTP. In addition, the $\pi-\pi$ interaction of F28 with GDP appears the open state of the GDP-bound K-Ras, while that of F28 with GTP is observed at the closed state of the GTP-bound K-Ras, which is hardly mentioned at the previous works, and this result also reveals binding difference of GDP and GTP to K-Ras. Therefore, based on the interaction network revealed by this work, a small molecule designed by imitating the interaction modes of GTP and GDP with K-Ras can potentially tune the activity of K-Ras and disturb binding of GNEFs.

■ CONCLUSIONS

Oncogenic K-Ras is thought as an important target of anticancer drug design. Understanding molecular mechanism concerning conformational changes of K-Ras is of high

https://doi.org/10.1021/acs.jcim.0c01470
J. Chem. Inf. Model. 2021, 61, 1954−1969

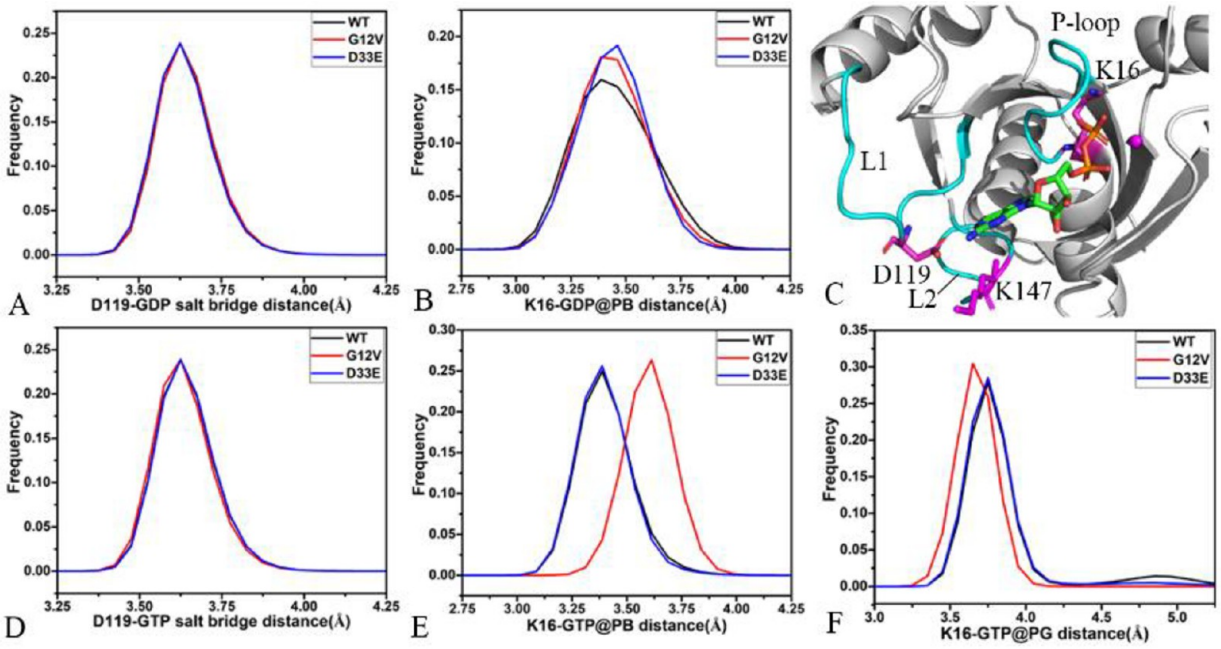

Figure 10. Salt bridge interactions of K16 and D119 with GDP and GTP: (A) the salt bridge between D119 and K16, (B) the salt bridge interaction of K16 with GDP, (C) two loops involved in the salt bridge interactions, (D) the salt bridge between D119 and GTP, and (E and F) two salt bridges formed between K16 and GTP.

Table 1. Hydrogen-Bonding Interactions of GDP with the WT and Mutated K-Ras

hydrogen bonds[a]		occupancy (%)[b]		
residues	GDP	WT	G12V	D33E
G13−N−H	O1B	87.4	93.7	97.8
V14−N−H	O2B	46.9	41.9	50.0
G15−N−H	O2B	98.1	98.4	98.9
K16−N−H	O2B	97.9	98.8	99.9
S17−N−H	O3B	72.3	64.9	93.9
A18−N−H	O2A	99.1	99.7	93.9
V29−O	O2*−H2*	41.4	42.1	25.3
D30−O	O3*−H3*	40.2	37.8	51.0
Y32−N−H	O*	29.8	9.4	2.2
N116−ND2−HD21	N7	82.9	82.5	84.9
K117−NZ−HZ1	O4*	42.1	39.8	40.2
S145−OG−HG	O6	61.9	62.9	69.6
A146−N−H	O6	71.2	71.2	69.1
K147	O6	71.2	71.9	75.4

[a]Hydrogen-bonding interactions are recognized by an acceptor··· donor distance of <3.5 Å and an acceptor···H−donor angle of >120°. [b]Occupancy (%) is defined as the percentage of simulation time that a specific hydrogen bond exists.

Table 2. Hydrogen-Bonding Interactions of GTP with the WT and Mutated K-Ras

hydrogen bonds[a]		occupancy (%)[b]		
residues	GTP	WT	G12V	D33E
G13−N−H	O1G	85.8	83.2	89.5
V14−N−H	O1B	30.2	31.5	31.3
G15−N−H	O1B	99.4	98.5	99.4
K16−N−H	O1B	99.9	99.9	99.9
S17−N−H	O2B	92.9	95.8	93.7
A18−N−H	O1A	99.8	99.7	99.8
V29−O	O2′−HO2′	36.2	17.2	15.1
D30−O	O3′−H3T	31.3	9.8	15.3
N116−ND2−HD21	N7	85.6	81.8	85.8
K117−NZ−HZ1	O4′	39.2	37.7	33.6
S145−OG−HG	N1	64.2	70.6	64.7
A146−N−H	O6	71.4	69.2	69.3
K147−N−H	O6	71.4	74.8	71.9

[a]Hydrogen-bonding interactions are recognized by an acceptor··· donor distance of <3.5 Å and an acceptor···H−donor angle of >120°. [b]Occupancy (%) is defined as the percentage of simulation time that a specific hydrogen bond exists.

significance for rational drug design toward oncogenic K-Ras. For this work, 2.4-μs MR-GaMD simulations of four replicas are performed on the GDP- and GTP-bound WT, G12V, and D33E K-Ras to enhance conformational sampling. Dynamics analysis and the calculated DCCMs suggest that G12V and D33E exceedingly affect the structural flexibility and motion modes of two switch domains SW1 and SW2 in the GDP- and GTP-associated K-Ras. Essential dynamics analysis uncovers that G12V and D33E change dynamics behavior of SW1 and SW2 compared to the GDP- and GTP-bound WT K-Ras. Free energy landscapes are constructed by using the distance of T35 away from E62 and RMSDs of backbone atoms as reaction coordinates and the results indicate that G12V and D33E not only alter free energy profiles of K-Ras but also induce the highly conformational disorder of the two switch domains, SW1 and SW2, in the GDP- and GTP-complexed K-Ras. Briefly, the changes in the structural flexibility, motion modes, dynamics behavior, and conformational orders of the two switch domains, SW1 and SW2, induced by G12V and D33E imply a possibility to tune the activity of K-Ras. The identified interaction networks of GDP and GTP with K-Ras show that the instability in hydrogen-bonding interactions of SW1 with GDP and GTP is a main cause for the highly conformational disorder of SW1 and SW2 in the WT and mutated states of K-Ras. We expect that this work can provide significantly

https://doi.org/10.1021/acs.jcim.0c01470
J. Chem. Inf. Model. 2021, 61, 1954−1969

theoretical hints and dynamics information for the design of clinically available anticancer inhibitors toward oncogenic K-Ras.

■ ASSOCIATED CONTENT

Supporting Information

The Supporting Information is available free of charge at https://pubs.acs.org/doi/10.1021/acs.jcim.0c01470.

Distances of magnesium ion (Mg^{2+}) away from the oxygen atoms of the phosphate groups in GTP and GDP; dynamics cross-correlation maps between residues; function of eigenvalues over eigenvectors arising from essential dynamics analysis; and representative structures of the GDP-associated WT K-Ras, the GTP-bound WT K-Ras, the GDP-bound G12V K-Ras, the GTP-bound G12V K-Ras, the GDP-associated D33E K-Ras, and the GTP-bound D33E K-Ras falling into the energy basins (PDF)

■ AUTHOR INFORMATION

Corresponding Authors

Jianzhong Chen − *School of Science, Shandong Jiaotong University, Jinan 250357, China;* orcid.org/0000-0003-1558-4398; Email: chenjianzhong1970@163.com, jzchen@sdjtu.edu.cn

Xinguo Liu − *School of Physics and Electronics, Shandong Normal University, Jinan 250358, China;* Email: liuxinguo@sdnu.edu.cn

Authors

Shaolong Zhang − *School of Physics and Electronics, Shandong Normal University, Jinan 250358, China*

Wei Wang − *School of Science, Shandong Jiaotong University, Jinan 250357, China*

Laixue Pang − *School of Science, Shandong Jiaotong University, Jinan 250357, China*

Qinggang Zhang − *School of Physics and Electronics, Shandong Normal University, Jinan 250358, China*

Complete contact information is available at: https://pubs.acs.org/10.1021/acs.jcim.0c01470

Notes

The authors declare no competing financial interest.

■ ACKNOWLEDGMENTS

This work is supported by the National Natural Science Foundation of China, Grants 11274205, 11274206, and 11504206, Shandong Provincial Natural Science Foundation (ZR2017MA040), and the Key Research and Development Project of Shandong Province (Nos. 2018GSF121014 and 2019GGX102050).

■ REFERENCES

(1) Spiegel, J.; Cromm, P. M.; Zimmermann, G.; Grossmann, T. N.; Waldmann, H. Small-molecule modulation of Ras signaling. *Nat. Chem. Biol.* **2014**, *10* (8), 613−622.

(2) Vetter, I. R.; Wittinghofer, A. The Guanine Nucleotide-Binding Switch in Three Dimensions. *Science* **2001**, *294* (5545), 1299−1304.

(3) Ma, J.; Karplus, M. Molecular switch in signal transduction: Reaction paths of the conformational changes in *ras* p21. *Proc. Natl. Acad. Sci. U. S. A.* **1997**, *94* (22), 11905−11910.

(4) Bourne, H. R.; Sanders, D. A.; McCormick, F. The GTPase superfamily: a conserved switch for diverse cell functions. *Nature* **1990**, *348* (6297), 125−132.

(5) Wennerberg, K.; Rossman, K. L.; Der, C. J. The Ras superfamily at a glance. *J. Cell Sci.* **2005**, *118* (5), 843−846.

(6) Lu, S.; Jang, H.; Muratcioglu, S.; Gursoy, A.; Keskin, O.; Nussinov, R.; Zhang, J. Ras Conformational Ensembles, Allostery, and Signaling. *Chem. Rev.* **2016**, *116* (11), 6607−6665.

(7) Lu, S.; Jang, H.; Gu, S.; Zhang, J.; Nussinov, R. Drugging Ras GTPase: a comprehensive mechanistic and signaling structural view. *Chem. Soc. Rev.* **2016**, *45* (18), 4929−4952.

(8) Araki, M.; Shima, F.; Yoshikawa, Y.; Muraoka, S.; Ijiri, Y.; Nagahara, Y.; Shirono, T.; Kataoka, T.; Tamura, A. Solution Structure of the State 1 Conformer of GTP-bound H-Ras Protein and Distinct Dynamic Properties between the State 1 and State 2 Conformers. *J. Biol. Chem.* **2011**, *286* (45), 39644−39653.

(9) Spoerner, M.; Hozsa, C.; Poetzl, J. A.; Reiss, K.; Ganser, P.; Geyer, M.; Kalbitzer, H. R. Conformational States of Human Rat Sarcoma (Ras) Protein Complexed with Its Natural Ligand GTP and Their Role for Effector Interaction and GTP Hydrolysis. *J. Biol. Chem.* **2010**, *285* (51), 39768−39778.

(10) Pálfy, G.; Vida, I.; Perczel, A. ^{1}H, ^{15}N backbone assignment and comparative analysis of the wild type and G12C, G12D, G12V mutants of K-Ras bound to GDP at physiological pH. *Biomol. NMR Assignments* **2020**, *14* (1), 1−7.

(11) Karnoub, A. E.; Weinberg, R. A. Ras oncogenes: split personalities. *Nat. Rev. Mol. Cell Biol.* **2008**, *9* (7), 517−531.

(12) Gorfe, A. A. Mechanisms of Allostery and Membrane Attachment in Ras GTPases: Implications for Anti-Cancer Drug Discovery. *Curr. Med. Chem.* **2010**, *17* (1), 1−9.

(13) Prior, I. A.; Lewis, P. D.; Mattos, C. A Comprehensive Survey of Ras Mutations in Cancer. *Cancer Res.* **2012**, *72* (10), 2457−2467.

(14) Hernández-Porras, I.; Schuhmacher, A. J.; Garcia-Medina, R.; Jiménez, B.; Cañamero, M.; de Martino, A.; Guerra, C. K-Ras^{V14I}-induced Noonan syndrome predisposes to tumour development in mice. *J. Pathol.* **2016**, *239* (2), 206−217.

(15) Lee, Y. S.; Bae, S. C. How do K-RAS-activated cells evade cellular defense mechanisms? *Oncogene* **2016**, *35* (7), 827−832.

(16) Jinesh, G. G.; Sambandam, V.; Vijayaraghavan, S.; Balaji, K.; Mukherjee, S. Molecular genetics and cellular events of K-Ras-driven tumorigenesis. *Oncogene* **2018**, *37* (7), 839−846.

(17) Downward, J. Targeting RAS signalling pathways in cancer therapy. *Nat. Rev. Cancer* **2003**, *3* (1), 11−22.

(18) Hunter, J. C.; Manandhar, A.; Carrasco, M. A.; Gurbani, D.; Gondi, S.; Westover, K. D. Biochemical and Structural Analysis of Common Cancer-Associated KRAS Mutations. *Mol. Cancer Res.* **2015**, *13* (9), 1325−1335.

(19) Poulin, E. J.; Bera, A. K.; Lu, J.; Lin, Y.-J.; Strasser, S. D.; Paulo, J. A.; Huang, T. Q.; Morales, C.; Yan, W.; Cook, J.; Nowak, J. A.; Brubaker, D. K.; Joughin, B. A.; Johnson, C. W.; DeStefanis, R. A.; Ghazi, P. C.; Gondi, S.; Wales, T. E.; Iacob, R. E.; Bogdanova, L.; Gierut, J. J.; Li, Y.; Engen, J. R.; Perez-Mancera, P. A.; Braun, B. S.; Gygi, S. P.; Lauffenburger, D. A.; Westover, K. D.; Haigis, K. M. Tissue-Specific Oncogenic Activity of KRAS^{A146T}. *Cancer Discovery* **2019**, *9* (6), 738−755.

(20) Parker, J. A.; Volmar, A. Y.; Pavlopoulos, S.; Mattos, C. K-Ras Populates Conformational States Differently from Its Isoform H-Ras and Oncogenic Mutant K-RasG12D. *Structure* **2018**, *26* (6), 810−820.e4.

(21) Fraser, J. S.; van den Bedem, H.; Samelson, A. J.; Lang, P. T.; Holton, J. M.; Echols, N.; Alber, T. Accessing protein conformational ensembles using room-temperature X-ray crystallography. *Proc. Natl. Acad. Sci. U. S. A.* **2011**, *108* (39), 16247−16252.

(22) Gentile, D. R.; Rathinaswamy, M. K.; Jenkins, M. L.; Moss, S. M.; Siempelkamp, B. D.; Renslo, A. R.; Burke, J. E.; Shokat, K. M. Ras Binder Induces a Modified Switch-II Pocket in GTP and GDP States. *Cell Chem. Biol.* **2017**, *24* (12), 1455−1466.e14.

(23) Spoerner, M.; Herrmann, C.; Vetter, I. R.; Kalbitzer, H. R.; Wittinghofer, A. Dynamic properties of the Ras switch I region and its

importance for binding to effectors. *Proc. Natl. Acad. Sci. U. S. A.* **2001**, *98* (9), 4944−4949.
(24) Hocker, H. J.; Cho, K.-J.; Chen, C.-Y. K.; Rambahal, N.; Sagineedu, S. R.; Shaari, K.; Stanslas, J.; Hancock, J. F.; Gorfe, A. A. Andrographolide derivatives inhibit guanine nucleotide exchange and abrogate oncogenic Ras function. *Proc. Natl. Acad. Sci. U. S. A.* **2013**, *110* (25), 10201−10206.
(25) Sakamoto, K.; Kamada, Y.; Sameshima, T.; Yaguchi, M.; Niida, A.; Sasaki, S.; Miwa, M.; Ohkubo, S.; Sakamoto, J.-i.; Kamaura, M.; Cho, N.; Tani, A. K-Ras(G12D)-selective inhibitory peptides generated by random peptide T7 phage display technology. *Biochem. Biophys. Res. Commun.* **2017**, *484* (3), 605−611.
(26) Cruz-Migoni, A.; Canning, P.; Quevedo, C. E.; Bataille, C. J. R.; Bery, N.; Miller, A.; Russell, A. J.; Phillips, S. E. V.; Carr, S. B.; Rabbitts, T. H. Structure-based development of new RAS-effector inhibitors from a combination of active and inactive RAS-binding compounds. *Proc. Natl. Acad. Sci. U. S. A.* **2019**, *116* (7), 2545−2550.
(27) Kaushik, A. C.; Wang, Y.-J.; Wang, X.; Wei, D.-Q. Irinotecan and vandetanib create synergies for treatment of pancreatic cancer patients with concomitant TP53 and KRAS mutations. *Briefings Bioinf.* **2020**, bbaa149.
(28) Johnson, C. W.; Lin, Y.-J.; Reid, D.; Parker, J.; Pavlopoulos, S.; Dischinger, P.; Graveel, C.; Aguirre, A. J.; Steensma, M.; Haigis, K. M.; Mattos, C. Isoform-Specific Destabilization of the Active Site Reveals a Molecular Mechanism of Intrinsic Activation of KRas G13D. *Cell Rep.* **2019**, *28* (6), 1538.
(29) Kunitski, M.; Eicke, N.; Huber, P.; Köhler, J.; Zeller, S.; Voigtsberger, J.; Schlott, N.; Henrichs, K.; Sann, H.; Trinter, F.; Schmidt, L. P. H.; Kalinin, A.; Schöffler, M. S.; Jahnke, T.; Lein, M.; Dörner, R. Double-slit photoelectron interference in strong-field ionization of the neon dimer. *Nat. Commun.* **2019**, *10* (1), 1.
(30) Bunda, S.; Heir, P.; Srikumar, T.; Cook, J. D.; Burrell, K.; Kano, Y.; Lee, J. E.; Zadeh, G.; Raught, B.; Ohh, M. Src promotes GTPase activity of Ras via tyrosine 32 phosphorylation. *Proc. Natl. Acad. Sci. U. S. A.* **2014**, *111* (36), E3785−E3794.
(31) Khaled, M.; Gorfe, A.; Sayyed-Ahmad, A. Conformational and Dynamical Effects of Tyr32 Phosphorylation in K-Ras: Molecular Dynamics Simulation and Markov State Models Analysis. *J. Phys. Chem. B* **2019**, *123* (36), 7667−7675.
(32) Ting, P. Y.; Johnson, C. W.; Fang, C.; Cao, X.; Graeber, T. G.; Mattos, C.; Colicelli, J. Tyrosine phosphorylation of RAS by ABL allosterically enhances effector binding. *FASEB J.* **2015**, *29* (9), 3750−3761.
(33) Prakash, P.; Litwin, D.; Liang, H.; Sarkar-Banerjee, S.; Dolino, D.; Zhou, Y.; Hancock, J. F.; Jayaraman, V.; Gorfe, A. A. Dynamics of Membrane-Bound G12V-KRAS from Simulations and Single-Molecule FRET in Native Nanodiscs. *Biophys. J.* **2019**, *116* (2), 179−183.
(34) Mazhab-Jafari, M. T.; Marshall, C. B.; Smith, M. J.; Gasmi-Seabrook, G. M. C.; Stathopulos, P. B.; Inagaki, F.; Kay, L. E.; Neel, B. G.; Ikura, M. Oncogenic and RASopathy-associated K-RAS mutations relieve membrane-dependent occlusion of the effector-binding site. *Proc. Natl. Acad. Sci. U. S. A.* **2015**, *112* (21), 6625−6630.
(35) Prakash, P.; Zhou, Y.; Liang, H.; Hancock, J. F.; Gorfe, A. A. Oncogenic K-Ras Binds to an Anionic Membrane in Two Distinct Orientations: A Molecular Dynamics Analysis. *Biophys. J.* **2016**, *110* (5), 1125−1138.
(36) Li, Z.; Buck, M. Computational Design of Myristoylated Cell-Penetrating Peptides Targeting Oncogenic K-Ras.G12D at the Effector-Binding Membrane Interface. *J. Chem. Inf. Model.* **2020**, *60* (1), 306−315.
(37) Lu, S.; Ni, D.; Wang, C.; He, X.; Lin, H.; Wang, Z.; Zhang, J. Deactivation Pathway of Ras GTPase Underlies Conformational Substates as Targets for Drug Design. *ACS Catal.* **2019**, *9* (8), 7188−7196.
(38) Ostrem, J. M.; Peters, U.; Sos, M. L.; Wells, J. A.; Shokat, K. M. K-Ras(G12C) inhibitors allosterically control GTP affinity and effector interactions. *Nature* **2013**, *503* (7477), 548−551.
(39) Johnson, C. W.; Reid, D.; Parker, J. A.; Salter, S.; Knihtila, R.; Kuzmic, P.; Mattos, C. The small GTPases K-Ras, N-Ras, and H-Ras have distinct biochemical properties determined by allosteric effects. *J. Biol. Chem.* **2017**, *292* (31), 12981−12993.
(40) Hunter, J. C.; Gurbani, D.; Ficarro, S. B.; Carrasco, M. A.; Lim, S. M.; Choi, H. G.; Xie, T.; Marto, J. A.; Chen, Z.; Gray, N. S.; Westover, K. D. In situ selectivity profiling and crystal structure of SML-8−73−1, an active site inhibitor of oncogenic K-Ras G12C. *Proc. Natl. Acad. Sci. U. S. A.* **2014**, *111* (24), 8895−8900.
(41) Hobbs, G. A.; Baker, N. M.; Miermont, A. M.; Thurman, R. D.; Pierobon, M.; Tran, T. H.; Anderson, A. O.; Waters, A. M.; Diehl, J. N.; Papke, B.; Hodge, R. G.; Klomp, J. E.; Goodwin, C. M.; DeLiberty, J. M.; Wang, J.; Ng, R. W. S.; Gautam, P.; Bryant, K. L.; Esposito, D.; Campbell, S. L.; Petricoin, E. F.; Simanshu, D. K.; Aguirre, A. J.; Wolpin, B. M.; Wennerberg, K.; Rudloff, U.; Cox, A. D.; Der, C. J. Atypical $KRAS^{G12R}$ Mutant Is Impaired in PI3K Signaling and Macropinocytosis in Pancreatic Cancer. *Cancer Discovery* **2020**, *10* (1), 104−123.
(42) Bera, A. K.; Lu, J.; Wales, T. E.; Gondi, S.; Gurbani, D.; Nelson, A.; Engen, J. R.; Westover, K. D. Structural basis of the atypical activation mechanism of $KRAS^{V14I}$. *J. Biol. Chem.* **2019**, *294* (38), 13964−13972.
(43) Bum-Erdene, K.; Liu, D.; Gonzalez-Gutierrez, G.; Ghozayel, M. K.; Xu, D.; Meroueh, S. O. Small-molecule covalent bond formation at tyrosine creates a binding site and inhibits activation of Ral GTPases. *Proc. Natl. Acad. Sci. U. S. A.* **2020**, *117* (13), 7131−7139.
(44) Kessler, D.; Gmachl, M.; Mantoulidis, A.; Martin, L. J.; Zoephel, A.; Mayer, M.; Gollner, A.; Covini, D.; Fischer, S.; Gerstberger, T.; Gmaschitz, T.; Goodwin, C.; Greb, P.; Häring, D.; Hela, W.; Hoffmann, J.; Karolyi-Oezguer, J.; Knesl, P.; Kornigg, S.; Koegl, M.; Kousek, R.; Lamarre, L.; Moser, F.; Munico-Martinez, S.; Peinsipp, C.; Phan, J.; Rinnenthal, J.; Sai, J.; Salamon, C.; Scherbantin, Y.; Schipany, K.; Schnitzer, R.; Schrenk, A.; Sharps, B.; Siszler, G.; Sun, Q.; Waterson, A.; Wolkerstorfer, B.; Zeeb, M.; Pearson, M.; Fesik, S. W.; McConnell, D. B. Drugging an undruggable pocket on KRAS. *Proc. Natl. Acad. Sci. U. S. A.* **2019**, *116* (32), 15823−15829.
(45) Canon, J.; Rex, K.; Saiki, A. Y.; Mohr, C.; Cooke, K.; Bagal, D.; Gaida, K.; Holt, T.; Knutson, C. G.; Koppada, N.; Lanman, B. A.; Werner, J.; Rapaport, A. S.; San Miguel, T.; Ortiz, R.; Osgood, T.; Sun, J.-R.; Zhu, X.; McCarter, J. D.; Volak, L. P.; Houk, B. E.; Fakih, M. G.; O'Neil, B. H.; Price, T. J.; Falchook, G. S.; Desai, J.; Kuo, J.; Govindan, R.; Hong, D. S.; Ouyang, W.; Henary, H.; Arvedson, T.; Cee, V. J.; Lipford, J. R. The clinical KRAS(G12C) inhibitor AMG 510 drives anti-tumour immunity. *Nature* **2019**, *575* (7781), 217−223.
(46) Hou, T.; Yu, R. Molecular Dynamics and Free Energy Studies on the Wild-type and Double Mutant HIV-1 Protease Complexed with Amprenavir and Two Amprenavir-Related Inhibitors: Mechanism for Binding and Drug Resistance. *J. Med. Chem.* **2007**, *50* (6), 1177−1188.
(47) Xue, W.; Yang, F.; Wang, P.; Zheng, G.; Chen, Y.; Yao, X.; Zhu, F. What Contributes to Serotonin−Norepinephrine Reuptake Inhibitors' Dual-Targeting Mechanism? The Key Role of Transmembrane Domain 6 in Human Serotonin and Norepinephrine Transporters Revealed by Molecular Dynamics Simulation. *ACS Chem. Neurosci.* **2018**, *9* (5), 1128−1140.
(48) Lin, X.; Gorfe, A. A. Transmembrane potential of physiologically relevant model membranes: Effects of membrane asymmetry. *J. Chem. Phys.* **2020**, *153* (10), 105103.
(49) Zhang, S.; Lin, X. Lipid Acyl Chain cis Double Bond Position Modulates Membrane Domain Registration/Anti-Registration. *J. Am. Chem. Soc.* **2019**, *141* (40), 15884−15890.
(50) Hu, G.; Ma, A.; Wang, J. Ligand Selectivity Mechanism and Conformational Changes in Guanine Riboswitch by Molecular Dynamics Simulations and Free Energy Calculations. *J. Chem. Inf. Model.* **2017**, *57* (4), 918−928.
(51) Xu, Y.; Li, S.; Yan, Z.; Ge, B.; Huang, F.; Yue, T. Revealing Cooperation between Knotted Conformation and Dimerization in

https://doi.org/10.1021/acs.jcim.0c01470
J. Chem. Inf. Model. 2021, 61, 1954−1969

Protein Stabilization by Molecular Dynamics Simulations. *J. Phys. Chem. Lett.* **2019**, *10* (19), 5815−5822.
(52) Wu, E. L.; Han, K.; Zhang, J. Z. H. Selectivity of Neutral/Weakly Basic P1 Group Inhibitors of Thrombin and Trypsin by a Molecular Dynamics Study. *Chem. - Eur. J.* **2008**, *14* (28), 8704−8714.
(53) Chen, J.; Wang, J.; Yin, B.; Pang, L.; Wang, W.; Zhu, W. Molecular Mechanism of Binding Selectivity of Inhibitors toward BACE1 and BACE2 Revealed by Multiple Short Molecular Dynamics Simulations and Free-Energy Predictions. *ACS Chem. Neurosci.* **2019**, *10* (10), 4303−4318.
(54) Lou, Z.; Li, P.; Han, K. Redox-Responsive Fluorescent Probes with Different Design Strategies. *Acc. Chem. Res.* **2015**, *48* (5), 1358−1368.
(55) Chen, J.; Liu, X.; Zhang, S.; Chen, J.; Sun, H.; Zhang, L.; Zhang, Q. Molecular mechanism with regard to the binding selectivity of inhibitors toward FABP5 and FABP7 explored by multiple short molecular dynamics simulations and free energy analyses. *Phys. Chem. Chem. Phys.* **2020**, *22* (4), 2262−2275.
(56) Zhang, Y.; Cao, Z.; Zhang, J. Z.; Xia, F. Double-Well Ultra-Coarse-Grained Model to Describe Protein Conformational Transitions. *J. Chem. Theory Comput.* **2020**, *16* (10), 6678−6689.
(57) Khan, M. T.; Ali, S.; Zeb, M. T.; Kaushik, A. C.; Malik, S. I.; Wei, D. Gibbs Free Energy Calculation of Mutation in PncA and RpsA Associated With Pyrazinamide Resistance. *Front. Mol. Biosci.* **2020**, *7*, 52.
(58) Song, D.; Luo, R.; Chen, H.-F. The IDP-Specific Force Field ff14IDPSFF Improves the Conformer Sampling of Intrinsically Disordered Proteins. *J. Chem. Inf. Model.* **2017**, *57* (5), 1166−1178.
(59) Barducci, A.; Bonomi, M.; Parrinello, M. Metadynamics. *Wiley Interdiscip. Rev.: Comput. Mol. Sci.* **2011**, *1* (5), 826−843.
(60) Sun, H.; Chen, P.; Li, D.; Li, Y.; Hou, T. Directly Binding Rather than Induced-Fit Dominated Binding Affinity Difference in (S)- and (R)-Crizotinib Bound MTH1. *J. Chem. Theory Comput.* **2016**, *12* (2), 851−860.
(61) Amadei, A.; Linssen, A. B. M.; Berendsen, H. J. C. Essential dynamics of proteins. *Proteins: Struct., Funct., Genet.* **1993**, *17* (4), 412−425.
(62) Pierce, L. C. T.; Salomon-Ferrer, R.; Augusto F. de Oliveira, C.; McCammon, J. A.; Walker, R. C. Routine Access to Millisecond Time Scale Events with Accelerated Molecular Dynamics. *J. Chem. Theory Comput.* **2012**, *8* (9), 2997−3002.
(63) Chen, J.; Yin, B.; Wang, W.; Sun, H. Effects of Disulfide Bonds on Binding of Inhibitors to β-Amyloid Cleaving Enzyme 1 Decoded by Multiple Replica Accelerated Molecular Dynamics Simulations. *ACS Chem. Neurosci.* **2020**, *11* (12), 1811−1826.
(64) Miao, Y.; Feher, V. A.; McCammon, J. A. Gaussian Accelerated Molecular Dynamics: Unconstrained Enhanced Sampling and Free Energy Calculation. *J. Chem. Theory Comput.* **2015**, *11* (8), 3584−3595.
(65) Wang, J.; Miao, Y. Mechanistic Insights into Specific G Protein Interactions with Adenosine Receptors. *J. Phys. Chem. B* **2019**, *123* (30), 6462−6473.
(66) Wang, J.; Alekseenko, A.; Kozakov, D.; Miao, Y. Improved Modeling of Peptide-Protein Binding Through Global Docking and Accelerated Molecular Dynamics Simulations. *Front. Mol. Biosci.* **2019**, *6*, 112.
(67) Wang, J.; Miao, Y. Peptide Gaussian accelerated molecular dynamics (Pep-GaMD): Enhanced sampling and free energy and kinetics calculations of peptide binding. *J. Chem. Phys.* **2020**, *153* (15), 154109.
(68) Chen, J.; Wang, W.; Sun, H.; Pang, L.; Yin, B. Mutation-mediated influences on binding of anaplastic lymphoma kinase to crizotinib decoded by multiple replica Gaussian accelerated molecular dynamics. *J. Comput.-Aided Mol. Des.* **2020**, *34* (12), 1289−1305.
(69) Vatansever, S.; Erman, B.; Gümüş, Z. H. Oncogenic G12D mutation alters local conformations and dynamics of K-Ras. *Sci. Rep.* **2019**, *9* (1), 11730.
(70) Pantsar, T.; Rissanen, S.; Dauch, D.; Laitinen, T.; Vattulainen, I.; Poso, A. Assessment of mutation probabilities of KRAS G12 missense mutants and their long-timescale dynamics by atomistic molecular simulations and Markov state modeling. *PLoS Comput. Biol.* **2018**, *14* (9), e1006458.
(71) Lukman, S.; Grant, B. J.; Gorfe, A. A.; Grant, G. H.; McCammon, J. A. The Distinct Conformational Dynamics of K-Ras and H-Ras A59G. *PLoS Comput. Biol.* **2010**, *6* (9), e1000922.
(72) Sayyed-Ahmad, A.; Prakash, P.; Gorfe, A. A. Distinct dynamics and interaction patterns in H- and K-Ras oncogenic P-loop mutants. *Proteins: Struct., Funct., Genet.* **2017**, *85* (9), 1618−1632.
(73) Lu, S.; Jang, H.; Nussinov, R.; Zhang, J. The Structural Basis of Oncogenic Mutations G12, G13 and Q61 in Small GTPase K-Ras4B. *Sci. Rep.* **2016**, *6* (1), 21949.
(74) Chen, J.; Wang, W.; Pang, L.; Zhu, W. Unveiling conformational dynamics changes of H-Ras induced by mutations based on accelerated molecular dynamics. *Phys. Chem. Chem. Phys.* **2020**, *22* (37), 21238−21250.
(75) Gorfe, A. A.; Grant, B. J.; McCammon, J. A. Mapping the Nucleotide and Isoform-Dependent Structural and Dynamical Features of Ras Proteins. *Structure* **2008**, *16* (6), 885−896.
(76) Xu, S.; Long, B. N.; Boris, G. H.; Chen, A.; Ni, S.; Kennedy, M. A. Structural insight into the rearrangement of the switch I region in GTP-bound G12A K-Ras. *Acta Crystallogr. D Struct. Biol.* **2017**, *73* (12), 970−984.
(77) Salomon-Ferrer, R.; Case, D. A.; Walker, R. C. An overview of the Amber biomolecular simulation package. *WIREs Comput. Mol. Sci.* **2013**, *3* (2), 198−210.
(78) Case, D. A.; Cheatham, T. E., III; Darden, T.; Gohlke, H.; Luo, R.; Merz, K. M., Jr.; Onufriev, A.; Simmerling, C.; Wang, B.; Woods, R. J. The Amber biomolecular simulation programs. *J. Comput. Chem.* **2005**, *26* (16), 1668−1688.
(79) Anandakrishnan, R.; Aguilar, B.; Onufriev, A. V. H++ 3.0: automating pK prediction and the preparation of biomolecular structures for atomistic molecular modeling and simulations. *Nucleic Acids Res.* **2012**, *40* (W1), W537−W541.
(80) Maier, J. A.; Martinez, C.; Kasavajhala, K.; Wickstrom, L.; Hauser, K. E.; Simmerling, C. ff14SB: Improving the Accuracy of Protein Side Chain and Backbone Parameters from ff99SB. *J. Chem. Theory Comput.* **2015**, *11* (8), 3696−3713.
(81) Meagher, K. L.; Redman, L. T.; Carlson, H. A. Development of polyphosphate parameters for use with the AMBER force field. *J. Comput. Chem.* **2003**, *24* (9), 1016−1025.
(82) Jorgensen, W. L.; Chandrasekhar, J.; Madura, J. D.; Impey, R. W.; Klein, M. L. Comparison of simple potential functions for simulating liquid water. *J. Chem. Phys.* **1983**, *79* (2), 926−935.
(83) Åqvist, J. Ion-water interaction potentials derived from free energy perturbation simulations. *J. Phys. Chem.* **1990**, *94* (21), 8021−8024.
(84) Miao, Y.; Sinko, W.; Pierce, L.; Bucher, D.; Walker, R. C.; McCammon, J. A. Improved Reweighting of Accelerated Molecular Dynamics Simulations for Free Energy Calculation. *J. Chem. Theory Comput.* **2014**, *10* (7), 2677−2689.
(85) Ryckaert, J.-P.; Ciccotti, G.; Berendsen, H. J. C. Numerical integration of the cartesian equations of motion of a system with constraints: molecular dynamics of n-alkanes. *J. Comput. Phys.* **1977**, *23* (3), 327−341.
(86) Izaguirre, J. A.; Catarello, D. P.; Wozniak, J. M.; Skeel, R. D. Langevin stabilization of molecular dynamics. *J. Chem. Phys.* **2001**, *114* (5), 2090−2098.
(87) Essmann, U.; Perera, L.; Berkowitz, M. L.; Darden, T.; Lee, H.; Pedersen, L. G. A smooth particle mesh Ewald method. *J. Chem. Phys.* **1995**, *103* (19), 8577−8593.
(88) Salomon-Ferrer, R.; Götz, A. W.; Poole, D.; Le Grand, S.; Walker, R. C. Routine Microsecond Molecular Dynamics Simulations with AMBER on GPUs. 2. Explicit Solvent Particle Mesh Ewald. *J. Chem. Theory Comput.* **2013**, *9* (9), 3878−3888.
(89) Götz, A. W.; Williamson, M. J.; Xu, D.; Poole, D.; Le Grand, S.; Walker, R. C. Routine Microsecond Molecular Dynamics Simulations

with AMBER on GPUs. 1. Generalized Born. *J. Chem. Theory Comput.* **2012**, *8* (5), 1542−1555.
(90) Roe, D. R.; Cheatham, T. E. PTRAJ and CPPTRAJ: Software for Processing and Analysis of Molecular Dynamics Trajectory Data. *J. Chem. Theory Comput.* **2013**, *9* (7), 3084−3095.
(91) Humphrey, W.; Dalke, A.; Schulten, K. VMD: Visual molecular dynamics. *J. Mol. Graphics* **1996**, *14* (1), 33−38.
(92) Ichiye, T.; Karplus, M. Collective motions in proteins: A covariance analysis of atomic fluctuations in molecular dynamics and normal mode simulations. *Proteins: Struct., Funct., Genet.* **1991**, *11* (3), 205−217.
(93) Chen, J.; Wang, X.; Zhu, T.; Zhang, Q.; Zhang, J. Z. H. A Comparative Insight into Amprenavir Resistance of Mutations V32I, G48V, I50V, I54V, and I84V in HIV-1 Protease Based on Thermodynamic Integration and MM-PBSA Methods. *J. Chem. Inf. Model.* **2015**, *55* (9), 1903−1913.
(94) Chen, J.; Wang, X.; Pang, L.; Zhang, J. Z. H.; Zhu, T. Effect of mutations on binding of ligands to guanine riboswitch probed by free energy perturbation and molecular dynamics simulations. *Nucleic Acids Res.* **2019**, *47* (13), 6618−6631.
(95) Milburn, M.; Tong, L.; deVos, A.; Brunger, A.; Yamaizumi, Z.; Nishimura, S.; Kim, S. Molecular switch for signal transduction: structural differences between active and inactive forms of protooncogenic ras proteins. *Science* **1990**, *247* (4945), 939−945.
(96) Lu, J.; Bera, A. K.; Gondi, S.; Westover, K. D. KRAS Switch Mutants D33E and A59G Crystallize in the State 1 Conformation. *Biochemistry* **2018**, *57* (3), 324−333.
(97) Hall, B. E.; Yang, S. S.; Boriack-Sjodin, P. A.; Kuriyan, J.; Bar-Sagi, D. Structure-based Mutagenesis Reveals Distinct Functions for Ras Switch 1 and Switch 2 in Sos-catalyzed Guanine Nucleotide Exchange. *J. Biol. Chem.* **2001**, *276* (29), 27629−27637.
(98) Baussand, J.; Kleinjung, J. Specific Conformational States of Ras GTPase upon Effector Binding. *J. Chem. Theory Comput.* **2013**, *9* (1), 738−749.
(99) Spoerner, M.; Nuehs, A.; Ganser, P.; Herrmann, C.; Wittinghofer, A.; Kalbitzer, H. R. Conformational States of Ras Complexed with the GTP Analogue GppNHp or GppCH2p: Implications for the Interaction with Effector Proteins. *Biochemistry* **2005**, *44* (6), 2225−2236.
(100) Buhrman, G.; Holzapfel, G.; Fetics, S.; Mattos, C. Allosteric modulation of Ras positions Q61 for a direct role in catalysis. *Proc. Natl. Acad. Sci. U. S. A.* **2010**, *107* (11), 4931−4936.
(101) Fetics, S. K.; Guterres, H.; Kearney, B. M.; Buhrman, G.; Ma, B.; Nussinov, R.; Mattos, C. Allosteric Effects of the Oncogenic RasQ61L Mutant on Raf-RBD. *Structure* **2015**, *23* (3), 505−516.
(102) Nnadi, C. I.; Jenkins, M. L.; Gentile, D. R.; Bateman, L. A.; Zaidman, D.; Balius, T. E.; Nomura, D. K.; Burke, J. E.; Shokat, K. M.; London, N. Novel K-Ras G12C Switch-II Covalent Binders Destabilize Ras and Accelerate Nucleotide Exchange. *J. Chem. Inf. Model.* **2018**, *58* (2), 464−471.
(103) Rohrer, M.; Prisner, T. F.; Brügmann, O.; Käss, H.; Spoerner, M.; Wittinghofer, A.; Kalbitzer, H. R. Structure of the Metal−Water Complex in Ras·GDP Studied by High-Field EPR Spectroscopy and 31P NMR Spectroscopy. *Biochemistry* **2001**, *40* (7), 1884−1889.
(104) Spoerner, M.; Wittinghofer, A.; Kalbitzer, H. R. Perturbation of the conformational equilibria in Ras by selective mutations as studied by 31P NMR spectroscopy. *FEBS Lett.* **2004**, *578* (3), 305−310.
(105) Vatansever, S.; Erman, B.; Gümüş, Z. H. Comparative effects of oncogenic mutations G12C, G12V, G13D, and Q61H on local conformations and dynamics of K-Ras. *Comput. Struct. Biotechnol. J.* **2020**, *18*, 1000−1011.
(106) Buhrman, G.; Kumar, V. S. S.; Cirit, M.; Haugh, J. M.; Mattos, C. Allosteric Modulation of Ras-GTP Is Linked to Signal Transduction through RAF Kinase. *J. Biol. Chem.* **2011**, *286* (5), 3323−3331.
(107) Salentin, S.; Schreiber, S.; Haupt, V. J.; Adasme, M. F.; Schroeder, M. PLIP: fully automated protein−ligand interaction profiler. *Nucleic Acids Res.* **2015**, *43* (W1), W443−W447.
(108) Deng, W.-Q.; Sun, L.; Huang, J.-D.; Chai, S.; Wen, S.-H.; Han, K.-L. Quantitative prediction of charge mobilities of π-stacked systems by first-principles simulation. *Nat. Protoc.* **2015**, *10* (4), 632−642.

https://doi.org/10.1021/acs.jcim.0c01470
J. Chem. Inf. Model. 2021, 61, 1954−1969